Article:
Sanders, Kelly, Lin, Chia-Liang, Smith, Abigail J et al. (7 more authors) (2017) The structure and function of an RNA polymerase interaction domain in the PcrA/UvrD helicase. Nucleic Acids Research. ISSN: 0305-1048

https://doi.org/10.1093/nar/gkx074

The structure and function of an RNA polymerase interaction domain in the PcrA/UvrD helicase

Sanders, K.*[1], Lin, C-L.*[2], Smith, A.J.*[1], Cronin, N.[2], Fisher, G.[1], Eftychidis., V.[3], McGlynn, P.[3], Savery, N.J.[1], Wigley, D.B.[2] and Dillingham, M.S.[1#]

[1]DNA:Protein Interactions Unit, School of Biochemistry, Biomedical Sciences Building, University of Bristol, BS8 1TD, UK. [2]Institute of Cancer Research, Chester Beatty Laboratories, 237 Fulham Road, London SW3 6JB, UK and Section of Structural Biology, Department of Medicine, Imperial College London, South Kensington Campus, London SW7 2AZ, UK. [3]Department of Biology, University of York, Wentworth Way, York YO10 5DD, United Kingdom.

*First three authors contributed equally

#Corresponding author mark.dillingham@bristol.ac.uk

ABSTRACT

The PcrA/UvrD helicase functions in multiple pathways that promote bacterial genome stability including the suppression of conflicts between replication and transcription and facilitating the repair of transcribed DNA. The reported ability of PcrA/UvrD to bind and backtrack RNA polymerase (1,2) might be relevant to these functions, but the structural basis for this activity is poorly understood. In this work, we define a minimal RNA polymerase interaction domain in PcrA, and report its crystal structure at 1.5 Å resolution. The domain adopts a Tudor-like fold that is similar to other RNA polymerase interaction domains, including that of the prototype transcription-coupled repair factor Mfd. Removal or mutation of the interaction domain reduces the ability of PcrA/UvrD to interact with and to remodel RNA polymerase complexes *in vitro*. The implications of this work for our understanding of the role of PcrA/UvrD at the interface of DNA replication, transcription and repair are discussed.

INTRODUCTION

Helicases are ubiquitous, abundant and diverse enzymes playing a wide variety of different roles in cellular nucleic acid metabolism (3). Several superfamilies (SF) of these enzymes have been described on the basis of primary structure and SFI and II, which are non-hexameric helicases, are by far the largest groups (4). Bacterial cells typically encode several SFI enzymes that function in different genome replication, maintenance and expression pathways (5). Structural studies have shown that SFI enzymes share highly conserved core helicase domains responsible for ATP-dependent DNA translocation and unwinding, and that their targeting to different pathways is often achieved via the modular addition of different specificity domains, either flanking or inserted within the core helicase domains (6).

An interesting example is provided by the UvrD helicase (also annotated Helicase II, or PcrA in many gram positive bacteria including *Bacillus subtilis*) which has been implicated in nucleotide excision repair (NER), mismatch repair, homologous recombination and rolling circle replication mechanisms (7-13). This multi-functionality is reflected in the ability of UvrD/PcrA to interact physically and functionally with many different partner proteins including UvrB, MutL, MutS, RecA and RepC/D (13-20). We and others have recently shown that PcrA/UvrD also interacts with RNA polymerase (1,14,21), and this interaction could be important for the UvrD-dependent backtracking of stalled RNA polymerase (1). It was suggested that this activity helps to recruit the NER machinery to sites of UV damage, acting as an alternative pathway of transcription-coupled repair in addition to the well-characterised Mfd pathway (for reviews see (22-25)). This ability of UvrD to remodel RNAP-DNA complexes might also be relevant to the ability of

PcrA/UvrD to suppress conflicts between replication and transcription, a property it shares with the very closely related helicase Rep (although Rep does not interact with RNAP) (26-28). The extreme C-terminal region of PcrA/UvrD is important for interaction with both RNAP (14,29) and UvrB (30). However, despite its apparent role as a protein interaction hub that targets the helicase to physiological substrates, there is no clear phenotype established for removal of the C-terminal domain (CTD), and its structure has never been resolved. In thirteen structures of the PcrA/UvrD protein from various organisms, this region of the protein was either removed to aid crystallisation or is disordered in the final model (31-36) (**Supplementary Figure 1**).

In this report, we define a small folded RNA polymerase interaction domain in *Geobacillus stearothermophilus* PcrA and have solved its structure at high resolution. Based on its similarity to other Tudor-like domains, we identify conserved residues on its surface that are likely to be directly involved in the interaction with RNAP. Mutation of these residues, or the complete removal of the interaction domain, substantially reduces the ability of PcrA/UvrD to bind to RNAP and to remodel transcription elongation complexes *in vitro*.

MATERIALS AND METHODS

Protein expression and purification

His-tagged *E. coli* RNAP holoenzyme was purified as described (37). GreB protein was a gift from Terence Strick. Purified ParB protein was a gift from James Taylor. Biotinylated BSA protein was purchased from ThermoScientific. UvrD and UvrD^{K708A} were purified from BL21(DE3) cells transformed with pETDUET-UvrD (15) or pETDUET-UvrD^{K708A}, which was made from pETDUET-UvrD by site directed mutagenesis. Cells were grown at 37°C to an A_{600} of ~0.5 before being used to inoculate 1 litre of LB + 100 μg/ml ampicillin to an A_{600} of ~0.025. When cells reached an A_{600} of 0.2 they were transferred to 18°C and when the A_{600} reached ~0.5, 1 mM IPTG was added to induce protein expression. Cultures were then grown overnight at 18°C and the cells were harvested by centrifugation at 4°C. The cell pellet was resuspended in 20 ml of lysis buffer (20 mM Tris–HCl pH 8.3, 10% (v/v) glycerol, 200 mM NaCl, 5 mM EDTA pH 8.0, 0.5 mM EGTA pH 8.0, 1 mM DTT) containing 4 mg of lysozyme and incubated on ice for 30 minutes. 250 μl 4% sodium deoxycholate was added and cells were then incubated on ice for another 30 minutes. To increase the UvrD solubility, NaCl concentration was increased to ~450 mM by adding 1.2 ml 5 M NaCl and stirring for 15 min at 4°C. The cells were lysed by sonication and the soluble fraction was recovered by centrifugation. In order to precipitate the UvrD saturated ammonium sulphate was added gradually to the supernatant until 30% saturation was reached. The protein was allowed to precipitate for 1 hour in an ice waterbath and was recovered by centrifugation at 4000 rpm for 30 minutes. The pellet was resuspended in buffer (20 mM Tris–HCl pH 8.3, 20% (v/v) glycerol, 400 mM NaCl, 2 mM EDTA pH 8.0, 0.5 mM EGTA pH 8.0, 1 mM DTT) and was slowly diluted in buffer A (20 mM Tris–HCl pH 8.3, 20%

(v/v) glycerol, 1 mM EDTA pH 8.0, 0.5 mM EGTA pH 8.0 and 1 mM DTT) until the salt concentration was approximately 200 mM NaCl (or 100 mM for the $UvrD^{K708A}$ mutant). This was then loaded onto a 5 ml Heparin column (GE) on an ÄKTA FPLC. The protein was eluted from the column using a NaCl gradient in buffer A. Fractions containing the protein of interest were combined and diluted in buffer A until the salt concentration was approximately 200 mM NaCl (or 100 mM for the $UvrD^{K708A}$ mutant). Protein was loaded onto a 1 ml MonoQ column (GE) on an ÄKTA FPLC. The protein was eluted using a NaCl gradient in buffer A. Fractions containing only the protein of interest were dialysed at 4°C overnight against storage buffer (20 mM Tris–HCl pH 8.3, 200 mM KCl, 1mM EDTA pH 8.0, 2 mM DTT, 20% (v/v) glycerol). UvrDΔC was purified from BL21DE3 cells transformed with pETDUET-$UvrD_{1–647}$ as described (15).

Biotinylated PcrA and biotinylated PcrA-Ct (including residues 653-724 of the native protein) were produced using vectors and purification protocols that have been described previously (14). An equivalent vector for expression of biotinylated PcrA-sCt was created by deleting a short region of the PcrA-Ct construct. This yielded a vector for overexpression of the extreme C-terminal region of PcrA (residues 673-724) fused to an N-terminal AviTag sequence (MSG LND IFE AQK* IEW HEG GG; the asterisk indicates the position of the biotinylated lysine). This protein was overexpressed and purified using the same method as for the PcrA-Ct construct.

Constructs for the expression of the histidine-tagged PcrA C-terminus were produced by cloning synthetic DNA (Invitrogen) into the pET47b vector (Novagen). The PcrA-Ct construct expresses a protein with an N-terminal hexa-histidine tag fused via a 3C cleavable linker to residues 653-724 of *Geobacillus stearothermophilus* PcrA. The sequence of the tag is MAH HHH HHS AAL EVL FQG *PGG G where the asterisk indicates the position of 3C cleavage. The PcrA-sCt

construct only codes for residues 673 to 724 of the native PcrA protein, but is otherwise equivalent to PcrA-Ct. Point mutations were made in all of the above vectors using the QuikChange II kit (Invitrogen) and the constructs were verified by DNA sequencing (Sequencing service, University of Dundee). His-tagged PcrA-Ct and his-tagged PcrA-sCt were overexpressed in BL21(DE3) with appropriate antibiotics and harvested using the same protocol as for full length PcrA (14). Following sonication, the proteins were bound to a 5 ml HisTrap column (GE Healthcare) in a buffer containing 50 mM Tris-Cl, pH7.5 and 200 mM NaCl, and eluted over a 20 mM to 500 mM imidazole gradient. Where appropriate, the his-tag was removed with HRV 3C protease overnight at 4ºC (Thermo Scientific, manufacturer's instructions) while dialysing against a buffer containing 50 mM Tris-Cl, pH7.5, 1 mM EDTA, 200 mM NaCl and 20 mM imidazole. The cleaved protein was re-passed over the HisTrap column to remove HRV 3C protease contamination and PcrA S-Ct was collected in the flow-through. The cleaved (or uncleaved) protein was finally purified using a Superdex75 gel filtration column (GE Healthcare) in a buffer containing 50 mM Tris-Cl, pH7.5, 1 mM EDTA, 1 mM DTT and 200 mM NaCl. Peak fractions were pooled and concentrated using a 3 kDa cut-off spin concentration device. Where appropriate, removal of the tag was verified by separation using a 10-20% Tris-tricine gel by comparison with the his-tagged protein. The concentration of protein was determined by spectrophotometry using a theoretical extinction coefficient of 11000 $M^{-1}cm^{-1}$. The protein was snap frozen and stored at -80^{o}C in a buffer containing 50 mM Tris-Cl, pH7.5, 1 mM EDTA, 200 mM NaCl, 1 mM DTT and 10% glycerol.

Crystallization, structure determination and structure analysis.

The PcrA-sCt protein (with the his-tagged removed) was concentrated to 20 mg/ml in a buffer of 50 mM Tris (pH 7.5), 1 mM EDTA, 200 mM NaCl and 10% glycerol. Crystals were grown using the sitting-drop vapor diffusion method at 18°C by mixing 0.2 µl protein solution with 0.2 µl precipitant solution containing 3.5 M sodium formate pH 7.0. Crystals were harvested and frozen using the precipitant solution. A mercury derivative was prepared by soaking the crystals for 4 hours in cryosolution (3.5 M sodium formate pH 7.0) containing 10 mM ethyl mercury phosphate, and then freezing. X-ray diffraction data were collected at 100K using a Rigaku FR-X X-ray generator and PILATUS 300K detector. The data were processed and scaled using the HKL3000R program (38). A single mercury site was found by direct methods in SHELXD (39). Heavy-atom refinement and phasing (using SIRAS) were performed using SHARP (40). Solvent flipping and density modification were performed using SOLOMON (41) and Parrot (42), respectively. An initial model was built automatically using Buccaneer (43) and the final structure model was manually rebuilt using Coot (44) with refinement in Refmac (45) and Phenix (46). Diffraction data and refinement statistics are listed in Table 1, and the co-ordinates of the structure have been deposited at the PDB under ID code 5DMA. Figures showing the conservation of residues in PcrA mapped onto the structure were created using ConSurf (47) and PyMOL. The multiple sequence alignment was based on 150 unique sequences that were the most similar to the *G. stearothermophilus* PcrA C-terminus using the ConSurf default input settings.

Pulldown assays

Pulldown assays were performed as in previous work (14) using either streptavidin-coated magnetic beads (New England Biolabs) for biotin-tagged bait proteins or substituting Ni^{2+}-NTA

magnetic beads (New England Biolabs) for his-tagged bait proteins. Briefly, DNA/RNA-depleted extracts of *Bacillus subtilis* 168 were produced as described previously (14). *Bacillus subtilis* was chosen as the source for the bait proteins because the PcrA from this organism is highly similar (85%) to its orthologue from *G. stearothermophilus*, and because the annotated proteome is important for the proteomics analysis (below). Nevertheless, it should be noted that our pulldown experiments may be susceptible to false negatives because of the different *Bacillaceae* species used for bait and prey proteins. The prepared extracts were then used as the prey in pulldown experiments. Purified bait proteins were incubated at near saturating concentrations with magnetic beads to allow binding. The baited beads were washed and added to *B. subtilis* cell extracts to allow binding with partner proteins. The beads were separated from the cell extract and washed before bait and prey proteins were harvested from the beads by boiling in SDS-PAGE sample buffer. The pulldown experiments were analysed by SDS-PAGE followed by either western blotting with an anti-RNAP β antibody (8RB13, Abcam (48)), or by mass spectrometry. Details of sample preparation for mass spectrometry can be found in the **Supplementary Information**.

Construction of templates for *in vitro* transcription assays

Linear DNA templates for *in vitro* transcription reactions were constructed by PCR amplification from pSRT7A1 (49) using Pfu DNA polymerase. Templates containing the T7A1 promoter were amplified using the upstream primer 5′-ACCTGACGTCTAAGAAACC-3′ and the downstream primer 5′-ATTACTGGAGGGGATGGGG-3′ to produce a 236 bp product. On this template transcription can be stalled by nucleotide starvation at +20 by omitting UTP. Transcription can also be chased to the template end to produce a transcript of 60 nt. Linear

biotinylated DNA template was made in a similar manner using a 5′-biotinylated upstream primer and DNA templates were purified using the QIAEX II DNA extraction kit (Qiagen). Plasmid pSRTB8B3+500 was created by inserting a 504 bp fragment amplified from the *E. coli rpoB* gene between the NcoI and XhoI sites located between the T7A1 promoter and the tandemly repeated BbvCI sites of pSRTB8B3 (50). On the resulting template transcription from the T7 promoter can be stalled at +20 by UTP starvation, or allowed to run to a downstream terminator to produce a 764 nt transcript. A biotinylated closed-circular plasmid template carrying a biotin-dT at position +585 on the transcribed strand was generated by annealing a biotin-dT-containing oligonucleotide into BbvCI-nicked plasmid pSRTB8B3+500, as described in (50).

***In vitro* transcription time course and transcript release assays**

For time course assays, transcription initiation complexes were formed by incubating 20 nM *E. coli* RNA polymerase holoenzyme with 2 ng/μl DNA template for 5 minutes at 37°C in repair buffer (40 mM HEPES, pH 8.0, 100 mM KCl, 8 mM $MgCl_2$, 4% glycerol (v/v), 5 mM DTT, 100 μg/ml BSA). Transcription elongation complexes stalled at +20 were then formed by nucleotide starvation: the preformed transcription initiation complexes were mixed with an equal volume of NTP stall mix in repair buffer (final concentrations 100 μ M ApU, 10 μM ATP, 10 μM GTP, 2 μM CTP, 0.5 μCi/μl [α -^{32}P] CTP) and incubated for 5 minutes at 37°C. Aliquots of the stalled elongation complexes were incubated with UvrD or its derivatives at the concentrations indicated for 5 minutes at 37°C. Transcription elongation was then allowed to continue for 5 minutes at 37°C by adding a "chase" of 100 μM NTPs, together with 10 μg/ml rifamipicin to ensure that only a single round of transcription took place. Reactions were stopped with an equal volume of

urea stop mix (7 M urea, 10 mM EDTA, 1% SDS, 2 x TBE, 0.05% bromophenol blue, 0.05% xylene cyanol). Samples were heated for 3 minutes at 90°C and resolved on a 15% polyacrylamide/7 M urea denaturing gel. Gels were analysed using a Molecular Dynamics Typhoon PhosphorImager and ImageQuant software. For comparison of RNAP remodelling activity as shown in Figure 5, the data were normalized across multiple gels by determining the total intensity of the remodelling products for any given protein at any given timepoint (see black bar in Figure 5A) and dividing this value by the highest value observed for the wild type activity on each gel (typically the final timepoint). This value therefore represents a relative remodelling activity compared to maximal wild type activity. The error bars represent the standard error of the mean for wild type (six experiments) or mutant UvrD (four experiments each) respectively.

For transcript release assays, stalled transcription elongation complexes were formed as described above, but using biotinylated template DNA. DNA containing the stalled complexes was bound to streptavidin paramagnetic beads (NEB) by incubating each reaction with beads taken from an equal volume of bead suspension (and washed twice with repair buffer) for 10 minutes at 20°C. The beads were then washed three times in equal volumes of repair buffer to remove unbound DNA and RNAP. 1 µM UvrD or UvrDΔC was added to 20 µl aliquots of the reaction where indicated and reactions were incubated for 5 minutes at 37°C. Transcription reactions were chased by adding 100 µM NTPs and 10 µg/ml rifamipicin for 5 minutes at 37°C. A magnet was used to separate pellet and supernatant fractions and the supernatant was added to 20 µl urea stop mix (fraction S). The pellet was resuspended in 20 µl repair buffer and added to 20 µl urea stop mix (fraction P).

For transcript-release experiments in which backtracking was analysed with GreB, reaction volumes were scaled up and 1 μM UvrD or its derivatives were added to 100 μl aliquots containing stalled transcription elongation complexes. Transcription reactions were chased as described above. A magnet was used to separate pellet and supernatant fractions and 20 μl of the supernatant was added to 20 μl urea stop mix (fraction S). The beads were resuspended in 80 μl repair buffer and a 20 μl sample was added to 20 μl urea stop mix (fraction P). The remainder of the bead suspension was split into 20 μl aliquots. 1 μM GreB was added where indicated and reactions were incubated for 5 minutes at 37°C. Then 100 μM NTPs were added where indicated and reactions were incubated for 5 minutes at 37°C. Reactions were stopped with 20 μl urea stop mix. Samples were heated for 3 minutes at 90°C and resolved on a 15% polyacrylamide/7 M urea denaturing gel. Gels were analysed using a Molecular Dynamics Typhoon in PhosphorImager mode and ImageQuant software.

ATPase assays

The ATPase activity of UvrD and its derivatives was measured using an enzyme linked assay in which ATP hydrolysis is coupled to NADH oxidation essentially as reported previously (51). However, ATPase assays were modified in that reactions were carried out at 37°C using 1 nM UvrD, 2 mM ATP and 2 μM ssDNA (47 nt). The ATPase activity of PcrA and its derivatives was measured using the same linked assay, according to the method described in (34).

TFO displacement (DNA translocase) assays

TFO assays were carried out essentially as described in (49). Assays were carried out on a linear plasmid template, pSRTB2EV, a derivative of pSRTB2 (50), in which an EcoRV site had been

introduced downstream of the TFO binding site by site-directed mutagenesis. This template was linearised by EcoRV, creating a blunt end 33 bp downstream of the triplex end. Assays were performed in repair buffer and the TFO containing DNA template was incubated with 1 μM UvrD or its derivatives and 100 μM NTP mix. 0.25 mg/ml Proteinase K and 10 mM $CaCl_2$ were added to the GSMB stop buffer and reactions were incubated for 30 minutes at 20°C before loading onto the gel to eliminate bandshifting by UvrD.

RESULTS

Structure of a Tudor-like RNA polymerase interaction domain in PcrA

We have shown previously that the CTD of *G. stearothermophilus* PcrA (PcrA-Ct; residues 653-724) is necessary and sufficient for interaction with RNA polymerase using affinity pulldown assays from extracts of *Bacillus subtilis* (14) (see **Supplementary Figure 1**). Secondary structure predictions using Jpred (52) suggested that this region of the protein includes a significant region of natively disordered protein that is poorly conserved. However, this is followed by a very highly conserved region that is predicted to consist entirely of beta-sheet (residues 673-724). Furthermore, the domain identification algorithms Ginzu (53) and Phyre2 (54) both predict that this beta-sheet region will fold into a Tudor-like domain. Despite very low primary structure homology, these algorithms identify RapA and CarD respectively as templates for homology modelling. Interestingly, these are both bacterial RNAP interaction partners containing conserved Tudor-like domains (55,56). Therefore, we hypothesized that the extreme C-terminus of PcrA adopts a Tudor fold and that this interacts directly with RNA polymerase. To test this idea, we designed a new shorter version of the PcrA CTD using the homology models as a guide. This construct, which we call PcrA-short Ct (PcrA-sCt), includes residues 673-724 of the native PcrA protein. Moreover, to produce the CTD of PcrA in greater quantities than we had achieved previously using a biotin-tag (14), we engineered plasmids for expression of PcrA-Ct and PcrA-sCt with a cleavable histidine tag at the N-terminus. Using this system, we were able to obtain large amounts of highly pure protein either with or without the tag (**Supplementary Figure 2**). To confirm that the shorter CTD construct retained the ability to interact with RNAP, we performed affinity pulldown experiments using the his-tagged PcrA-sCt protein as bait and

nucleic acid-depleted cell extracts as prey (14). As expected, the original PcrA-Ct construct efficiently pulled down RNA polymerase from a *Bacillus subtilis* extract in a dose-dependent manner. In agreement with our hypothesis, the shorter PcrA-sCt construct retained the ability to pulldown RNAP, and the efficiency was comparable to PcrA-Ct (**Supplementary Figure 2**). For reasons that will be discussed below, we also investigated whether the PcrA CTD was able to bind to DNA. However, no interaction between the PcrA CTD and either single- or double-stranded DNA was detected using gel shift assays (**Supplementary Figure 3**).

Crystals of PcrA-sCt (with the histidine tag removed) were obtained using the sitting drop vapour diffusion method. The structure was solved using a heavy atom derivative at a final resolution of 1.5Å (R_{free} = 22.2%) (**Figure 1**). The final model includes all of the residues of the native PcrA sequence (W673 to V724) and an N-terminal glycine from the tag linker region. As predicted, the extreme C-terminal region of PcrA adopts a Tudor-like fold consisting of 5 anti-parallel beta strands that form a twisted β sheet. It closely resembles other bacterial Tudor domains such as those found in RapA, CarD and Mfd (**Figure 2**) (57-61). A search with DALI (62) also reveals strong similarity to NusG (63) and to eukaryotic "histone readers" including PHF1 (64). These histone readers are responsible for the recognition of methylated lysine residues in chromatin. Many structures of Tudor domains interacting with their partner proteins or peptides have shown that one particular face of the fold is often responsible for the interaction (65), although there are apparent exceptions including RapA (59) (**Figure 2**). In histone readers, this face includes an "aromatic cage" that typically accepts the methylated side chain of a lysine residue. Interestingly, some key residues that form this aromatic cage appear to be equivalent in PcrA (eg W684, F705). However, PcrA also features a charged lysine residue (K712) in this

region. Although not common for Tudor domains in general, this lysine residue is strongly conserved within PcrA/UvrD orthologues (Figure 1D). We were especially interested to compare our structure with the complex of the Mfd Tudor domain bound to RNA polymerase, because PcrA/UvrD has been reported to function in an alternative TCR pathway (1). The structure of *Thermus thermophilus* Mfd bound to RNAP shows that it binds to the so-called β1 region (60) and this is also true of the Tudor domain found in *Mycobacterium tuberculosis* CarD (58,61). In both of those structures, the Tudor domain forms a continuous anti-parallel beta-sheet with the partner protein, which is further stabilised by side-chain interactions. Conserved residues that are important for interaction with RNAP include a lysine residue (K360 in *T. thermophilus* Mfd) that is somewhat similarly positioned to the aforementioned K712 in PcrA (57). However, it should be noted that there is no apparent sequence homology between the Tudor-like domains of PcrA and Mfd.

Conserved amino acids required for binding RNA polymerase

Several highly conserved residues cluster together on the surface of the PcrA Tudor fold that frequently forms a protein:protein interface in other systems (**Figures 1 and 2**). We reasoned that these residues might be directly involved in the interaction with RNA polymerase. To test this hypothesis, we individually mutated several of them (H681A, W684A, K712A and L714A) and tested the ability of the resulting CTD constructs to interact with RNAP in pulldown assays. The mutant PcrA-sCt proteins were purified using the same method as for wild type and their CD spectra were all characteristic of β sheet as expected, suggesting normal global folding (**Supplementary Figure 4**). The pulldown assays revealed that each of the single mutant proteins had a severely reduced ability to bind to RNAP (**Figure 1C**). Indeed, western blotting of

the gels with an anti-RNAP subunit antibody suggested the binding was marginally above a "no bait" control and comparable to a second negative control experiment using *B. subtilis* ParB (a protein not known to bind RNAP).

The K712A and L714A mutations were also made in the context of a full length biotinylated PcrA construct used in our previous studies. These mutant proteins displayed a greatly reduced ability to interact with RNAP, but the binding was reproducibly higher than background (**Figure 3A**). Moreover, as has been shown previously (14), the complete deletion of the CTD from the full length protein dramatically reduces binding to RNAP. In order to validate these experiments and to test for protein interactions of the CTD in an unbiased fashion, we also analysed the pulldown experiments using mass spectrometry. Relative quantification of prey proteins was performed by comparing total ion scores using the "no bait" pulldown as a control (**Figure 3B** and **Supplementary Table 1**). The relative ion score for the PcrA bait acts as an internal control, showing enrichment over control for full length constructs, and a reduced enrichment for the PcrA-Ct construct as would be expected based on the different polypeptide lengths. The results for the wild type PcrA bait reproduced our previously published experiments showing that it interacts with many proteins in the cell extract (see also (14) and **Supplementary Table 1** for full details). Prominently these include both core and accessory subunits of RNA polymerase (α, β, β′, δ, ω), as well as a variety of sigma factors. Other enriched proteins of interest include YvgS/HelD (a SF1 helicase also known to associate with RNAP), UvrB (a known PcrA binding partner involved in NER), DNA pol I (a DNA repair specific and bypass polymerase) and LigA (an NAD+-dependent DNA ligase originating from the same operon as PcrA) (**Figures 3B**). In good agreement with the western blotting analysis, mass spectrometry showed that mutation

(K712A or L714A) or removal of the PcrA CTD substantially reduced or almost eliminated the interaction with core RNAP subunits respectively. These data show that the mutated residues are critical for the RNAP binding function of the CTD, and that the apparent residual binding we have observed probably occurs at a different site in the PcrA protein. Interestingly, a concomitant reduction in several other interaction partners including UvrB and YvgS was also detected. This is consistent with two possibilities that cannot be distinguished based on these experiments. Either the CTD of PcrA is important for direct interaction with all of these proteins, or the other proteins are associated with the RNAP subunits that are pulled down by PcrA. In this respect it should be noted that PcrA/UvrD interacts directly with RNAP and UvrB (1,14,15), and that YvgS/HelD interacts directly with RNAP (66). In distinct contrast, the removal or mutation of the CTD of PcrA did not affect the apparent interaction with DNA pol I or LigA, whereas the CTD alone bound poorly to these proteins, showing that they must interact mainly with the N-terminal region of PcrA. Importantly, this observation confirms that the mutant PcrA proteins remain largely folded, as would be expected based on CD analysis of the CTD variants alone (see above). This assertion is further supported by analysis of the DNA-dependent ATPase activity, which is similar or slightly better than wild type for both mutant proteins (**Table 2**).

The UvrD CTD is important for the remodelling of RNAP transcripts

Due to differences in the manner in which it was discovered in the model organisms *B. subtilis* and *E. coli*, the helicase studied here is often annotated as PcrA in Gram-positive organisms and UvrD in Gram–negative organisms. It was therefore of considerable interest to us that *E. coli* UvrD was recently shown to induce backtracking of RNAP *in vitro*, causing it to slide backwards on the DNA and bringing about the displacement of the 3′ end of the RNA from the active site

(1). To reproduce this activity and to probe the potential role of the CTD, *in vitro* transcription reactions were performed in which wild type or mutant UvrD was incubated with RNAP (both from *E. coli*) that had been stalled 20 nt downstream of the T7A1 promoter by omission of UTP. The reaction was then "chased" with NTPs, and rifampicin was added to ensure single round conditions.

In initial experiments, both circular and linear DNA templates were used, and these were also biotinylated so that displacement of RNAP could be monitored by examining the release of the transcript into the supernatant using a pulldown approach (**Figure 4A**). In the absence of UvrD, the RNAP forms long transcripts indicative of processive transcription elongation (Figure 4B; lanes 2, 3, 7 and 8). Shorter RNA transcripts are formed in a UvrD-dependent manner regardless of whether the template is circular or linear, and these transcripts generally remain in the pellet fraction (**Figure 4B**). This is consistent with UvrD causing backtracking of RNAP as reported previously (1), and this was confirmed by adding the transcript cleavage factor GreB (which removes the extruding 3′ portion of the nascent RNA) and then chasing the reaction with NTPs to generate full length transcripts (**Supplementary Figure 5,** lanes 1-13, see Figure Legend for details). In addition to backtracking, we also observed efficient UvrD-dependent displacement of short RNA transcripts into the supernatant, and this phenomenon was only observed with the linear template (**Figure 4B,** see asterisks**)**. Interestingly, the size of these released transcripts is equivalent to the size of the major GreB-cleavage products (**Supplementary Figure 5,** compare lanes 9 and 11), which are indicative of favoured backtracking positions for RNAP on the template. In the absence of UvrD, several transcripts that are longer than the distance from the promoter to the end of the template were observed. Such transcripts result from transfer of

RNAP from the end of one DNA molecule to the start of another (67). Interestingly, addition of UvrD abolishes this end-to-end transfer, possibly by backtracking RNAP away from the DNA end, or by dissociating it from the DNA altogether. Together, these experiments show that UvrD is capable of remodeling transcription elongation complexes *in vitro*, by promoting both the reversible backtracking of RNAP, and the premature release of short RNA transcripts from linear templates.

We next performed experiments on free linear template DNA using mutant UvrD proteins in which the CTD was either removed or mutated (**Figure 5**). The very strong conservation of primary sequence in the CTD (**Supplementary Figure 1**) allows the facile design of mutations in *E. coli* UvrD (UvrDΔC or UvrD^{K708A}) that are equivalent to those we have studied in PcrA. In the absence of UvrD, RNAP transcribed the template DNA to produce products which correspond to transcription to the end of the template (**Figure 5A;** lane 1 +60). As expected, in the presence of wild type UvrD a series of shorter RNA transcripts were observed (**Figure 5A**, compare lane 1 with lanes 2-5). This effect was UvrD dose-dependent, but less efficient than has been reported previously (1). On these substrates, UvrD-dependent RNAP remodelling was substantially reduced in the absence of the CTD (**Figures 5A** and **5B**, compare lanes 2-5 with lanes 6-9). However, it was still possible to observe backtracking of RNAP on linear DNA templates using this mutant, especially when bound to streptavidin coated magnetic beads (**Supplementary Figure 5**). The deletion of the CTD is particularly effective at decreasing the premature release of RNA into solution that is observed on linear templates (**Figure 5A** and **Supplementary Figure 5**, see asterisks). Mutation of the highly conserved lysine in the CTD

(K708A) also reduced the remodeling of RNAP-RNA complexes relative to wild type, albeit not to the same extent as does the complete removal of the CTD (**Figures 5A and 5B**).

Together, these experiments indicate that the CTD is important but not essential for catalysing backtracking and RNA release from RNAP during transcription *in vitro*. To eliminate the possibility that the mutant proteins were simply unfolded, or that the observed remodeling defects reflected a reduced ability of the mutant proteins to move along DNA we assayed for ATPase and DNA translocase activity. These experiments showed that UvrD proteins in which the CTD had been either mutated or deleted retained ssDNA-dependent ATPase and translocase activities that were either comparable to, or even better than, wild type activity (**Table 2** and **Figure 5C**). This is broadly consistent with previous experiments on a UvrD protein with a 40 amino acid C-terminal deletion which displayed wild type ATPase and helicase activity (68).

DISCUSSION

Superfamily I helicases are highly abundant and often multi-functional enzymes playing diverse roles in bacterial nucleic acid metabolism. Interestingly, several recent studies have shown that these enzymes function at the interface of DNA replication, transcription and repair. In rapidly dividing bacterial cells the replication and transcription of DNA occur on the same template at the same time. Conflicts between the two systems are inevitable and can lead to genomic instability, and so cells have developed systems that either reduce their occurrence or minimise their impact (reviewed in (69)). For example, some Superfamily I helicases have been shown to help the replisome bypass physical barriers including transcription complexes in various model organisms. However, the mechanisms by which they do so are only recently becoming apparent and may vary widely. In *E. coli*, the SF1 helicases Rep, UvrD and DinG have all been shown to resolve replication:transcription conflicts (26,27,70). Rep functions as a component of the replisome itself, by associating with the replicative helicase DnaB, and loss of this interaction results in transcription:replication conflicts (26,71). In distinct contrast, UvrD interacts directly with RNA polymerase (1), and an equivalent interaction has also been demonstrated in the orthologous PcrA enzyme (14,21,72). However, recent work in *Bacillus subtilis* shows that deletion of the PcrA CTD does not affect its essential role in resolving replication:transcription conflicts, whereas elimination of its ATPase/helicase activity does (27). Although perhaps surprising, this result is consistent with the long standing observation that Rep and UvrD share an essential function in *E. coli* (73,74), despite the fact that Rep does not interact with RNA polymerase. Nevertheless, the extremely high conservation of the PcrA/UvrD CTD region would suggest either that there is some unappreciated complexity in observing a phenotype associated

with its deletion and/or that it has a different role that is also (presumably) related to transcription. Indeed, recent experiments have suggested that UvrD can backtrack RNA polymerase *in vitro* and *in vivo* (1,2). We have shown here that this backtracking function is perturbed, albeit not entirely eliminated, by deletion or mutation of the CTD. Therefore, this work potentially identifies separation of function mutants that can be used to study the backtracking role of PcrA/UvrD specifically (25). In this respect, it is interesting and important to note that the loss of the PcrA/UvrD CTD has no apparent effect on nucleotide excision repair, mismatch repair or the resolution of transcription:replication conflicts *in vivo* (see **Supplementary Figure 6** and accompanying legend) (15,27,68,75). This implies that efficient RNAP remodelling is not important for any of these processes, at least in certain circumstances. A key challenge for future experiments will be to rationalise how the extreme multi-functionality displayed by helicases like PcrA/UvrD relates to the spectrum of protein:protein interactions that they can form, and how these different aspects of their function are regulated.

We have further defined the minimal RNAP polymerase interaction domain in the C-terminal region using *G. stearothermophilus* PcrA as a model system. We have shown for the first time that this adopts a Tudor fold in common with several other bacterial proteins involved in modulating transcription. Removal of the CTD of PcrA causes either no reduction or a modest reduction in ATPase, helicase and translocase activity *in vitro* (14,32). A similar analysis of UvrD showed no change in translocase activity and either no change or a moderate increase in ATPase (this work and (15,68,75)) Moreover, our biochemical analysis shows that the isolated CTD of PcrA does not bind to either single- or double-stranded DNA (Supplementary Figure 3). Therefore, despite the location of this domain in the vicinity of the displaced strand during DNA

unwinding, it does not seem to be involved in directly stimulating helicase activity, and may even have an attenuating effect on the ATPase. Simple point mutations in the CTD of PcrA greatly reduce RNAP binding but have no significant effect on the ssDNA-dependent ATPase activity. These mutations map to a well-conserved surface on the CTD of PcrA/UvrD orthologues. It is noteworthy that the same region of the Tudor fold is frequently observed to be the interaction interface for many other Tudor domains that are quite diverse at the level of primary structure. Given that Tudor domains are well-characterised as readers of methylated lysines in eukaryotic chromatin, a highly speculative possibility is that PcrA/UvrD might interact with RNAP following post-translational modifications of lysines or arginines. These are abundant in bacterial proteins including RNAP but their function is usually unclear (76,77).

We do not know precisely where the CTD of PcrA/UvrD engages RNA polymerase. Two-hybrid data and far western blots have suggested that the PcrA CTD contacts the N-terminal region (aa 1-400) of the β subunit (29). Given that related Tudor domains in Mfd and CarD/CdnL family proteins make contact with the β1 region (which is found within aa 1-400), an intriguing possibility is that PcrA/UvrD and Mfd compete for the same interaction patch on RNAP. However, we do not currently favour this possibility because we do not observe a dominant negative effect of the CTD upon Mfd function *in vitro* (data not shown). It is also quite possible that the C-terminal Tudor domain is not the only determinant of the RNAP interaction, and feasible that the details of the interaction differ between the UvrD and PcrA proteins studied here. Such factors would complicate the interpretation of any phenotypic analysis, and might also explain why the PcrA/UvrD mutants used in this study retain a limited ability to bind or backtrack RNA polymerase. Indeed, far western blots have suggested that an additional region in

the N-terminus of PcrA is important for an interaction with the β′ subunit of RNAP in *Bacillus subtilis* (29). Moreover, crosslinking experiments with *E. coli* UvrD and RNAP also suggest an interface involving the N-terminal helicase region (1). Further support for a more extensive interface is provided by analogy with RapA. A structure of RapA bound to RNAP shows that, although its Tudor domains are important for the inter-protein interactions as expected, the entire RapA protein including the core helicase regions also plays a role in the interactions (59). A final complexity is that the interaction could be modulated by a regulatory signal. For example, the ability of UvrD to backtrack RNAP has recently been shown to be enhanced by the presence of the small molecule alarmone ppGpp: this effect is likely due in part to changes in the properties of RNAP, but may also reflect an altered interaction between UvrD and RNAP (2). These questions will be the subject of further study.

FUNDING

This work was supported by the BBSRC (BB/I003142/1 to MD and NS and BB/I001859/2 to PG), the Wellcome Trust (077368 and 100401 to MD; 095519 to DW), the MRC (MR/N009258/1 to DW), and CRUK (C6913/A12799 to DW).

ACKNOWLEDGEMENTS

We are grateful to Dek Woolfson and his group for access and advice on the use of CD spectroscopy, Kate Heesom for expert technical assistance with mass spectrometry, and to Terence Strick and James Taylor for their kind gifts of purified proteins. We also thank Emma Gwynn, Sinead O'Hara, Madeleine Smith and Jennifer Gurnett for preliminary experimental observations that were relevant to this work.

Table 1. X-ray data collection and refinement statistics for PcrA-sCt

	Hg	Native
Data collection statistics		
Wavelength (Å)	1.54	1.54
Space group	$P3_221$	$P3_221$
Cell dimensions (a, b, c) (Å)	50.4, 50.4, 40.4	50.5, 50.5, 40.2
Resolution (Å)	50-1.7 (1.8-1.7)*	50–1.5 (1.6–1.5)*
Observed/unique reflections	41952/6980	92776/9252
Data redundancy	6.0 (3.0)	10.0 (5.1)
Completeness (%)	99.3 (98.7)	99.9 (98.9)
Rsym (%)	7.5 (15.8)	3.4 (18.5)
$I/\sigma(I)$	33.6 (8.1)	61.6 (7.7)
Refinement statistics		
Resolution range (Å)		30.0–1.5
Reflections (work/test)		9167/438
R_{work}/R_{free} (%)		19.5/22.2
Number of atoms (protein/water)		407/65
Average B-factor (protein/solvent) ($Å^2$)		15.2/25.5
RMSD in bond length (Å)/bond angle (°)		0.007/1.193

*Values in parentheses refer to the highest resolution shell.

Table 2. ssDNA-dependent ATPase activity of PcrA and UvrD

Protein	**ATPase (s^{-1})[a]**
Wild type PcrA	12.1 ± 0.8
PcrA K712A	15.8 ± 0.7
PcrA L714A	18.9 ± 1.8
Wild type UvrD	81.1 ± 3.0
UvrDΔC	194.9 ± 7.5
UvrD K708A	82.8± 19.8

a. ATP hydrolysis was measured using a coupled assay as described in the Materials and Methods under conditions of saturating ATP and ssDNA. The values reported are the mean turnover number and the standard error of the mean for three independent experiments.

References

1. Epshtein, V., Kamarthapu, V., McGary, K., Svetlov, V., Ueberheide, B., Proshkin, S., Mironov, A. and Nudler, E. (2014) UvrD facilitates DNA repair by pulling RNA polymerase backwards. *Nature*, **505**, 372-377.
2. Kamarthapu, V., Epshtein, V., Benjamin, B., Proshkin, S., Mironov, A., Cashel, M. and Nudler, E. (2016) ppGpp couples transcription to DNA repair in E. coli. *Science*, **352**, 993-996.
3. Singleton, M.R., Dillingham, M.S. and Wigley, D.B. (2007) Structure and mechanism of helicases and nucleic acid translocases. *Annu Rev Biochem*, **76**, 23-50.
4. Fairman-Williams, M.E., Guenther, U.P. and Jankowsky, E. (2010) SF1 and SF2 helicases: family matters. *Curr Opin Struct Biol*, **20**, 313-324.
5. Gilhooly, N.S., Gwynn, E.J. and Dillingham, M.S. (2013) Superfamily 1 helicases. *Front Biosci (Schol Ed)*, **5**, 206-216.
6. Dillingham, M.S. (2011) Superfamily I helicases as modular components of DNA-processing machines. *Biochem Soc Trans*, **39**, 413-423.
7. Iyer, R.R., Pluciennik, A., Burdett, V. and Modrich, P.L. (2006) DNA mismatch repair: functions and mechanisms. *Chem Rev*, **106**, 302-323.
8. Reardon, J.T. and Sancar, A. (2005) Nucleotide excision repair. *Prog Nucleic Acid Res Mol Biol*, **79**, 183-235.
9. Washburn, B.K. and Kushner, S.R. (1991) Construction and analysis of deletions in the structural gene (uvrD) for DNA helicase II of Escherichia coli. *J Bacteriol*, **173**, 2569-2575.
10. Arthur, H.M. and Lloyd, R.G. (1980) Hyper-recombination in uvrD mutants of Escherichia coli K-12. *Mol Gen Genet*, **180**, 185-191.
11. Zieg, J., Maples, V.F. and Kushner, S.R. (1978) Recombinant levels of Escherichia coli K-12 mutants deficient in various replication, recombination, or repair genes. *J Bacteriol*, **134**, 958-966.
12. Bruand, C. and Ehrlich, S.D. (2000) UvrD-dependent replication of rolling-circle plasmids in Escherichia coli. *Mol Microbiol*, **35**, 204-210.
13. Iordanescu, S. (1993) Plasmid pT181-linked suppressors of the Staphylococcus aureus pcrA3 chromosomal mutation. *J Bacteriol*, **175**, 3916-3917.
14. Gwynn, E.J., Smith, A.J., Guy, C.P., Savery, N.J., McGlynn, P. and Dillingham, M.S. (2013) The conserved C-terminus of the PcrA/UvrD helicase interacts directly with RNA polymerase. *PLoS One*, **8**, e78141.
15. Manelyte, L., Guy, C.P., Smith, R.M., Dillingham, M.S., McGlynn, P. and Savery, N.J. (2009) The unstructured C-terminal extension of UvrD interacts with UvrB, but is dispensable for nucleotide excision repair. *DNA Repair (Amst)*, **8**, 1300-1310.
16. Atkinson, J., Guy, C.P., Cadman, C.J., Moolenaar, G.F., Goosen, N. and McGlynn, P. (2009) Stimulation of UvrD helicase by UvrAB. *J Biol Chem*, **284**, 9612-9623.
17. Matson, S.W. and Robertson, A.B. (2006) The UvrD helicase and its modulation by the mismatch repair protein MutL. *Nucleic Acids Res*, **34**, 4089-4097.
18. Hall, M.C., Jordan, J.R. and Matson, S.W. (1998) Evidence for a physical interaction between the Escherichia coli methyl-directed mismatch repair proteins MutL and UvrD. *EMBO J*, **17**, 1535-1541.
19. Veaute, X., Delmas, S., Selva, M., Jeusset, J., Le Cam, E., Matic, I., Fabre, F. and Petit, M.A. (2005) UvrD helicase, unlike Rep helicase, dismantles RecA nucleoprotein filaments in Escherichia coli. *Embo J*, **24**, 180-189.
20. Machon, C., Lynch, G.P., Thomson, N.H., Scott, D.J., Thomas, C.D. and Soultanas, P. (2010) RepD-mediated recruitment of PcrA helicase at the Staphylococcus aureus pC221 plasmid replication origin, oriD. *Nucleic Acids Res*, **38**, 1874-1888.
21. Delumeau, O., Lecointe, F., Muntel, J., Guillot, A., Guedon, E., Monnet, V., Hecker, M., Becher, D., Polard, P. and Noirot, P. (2011) The dynamic protein partnership of RNA polymerase in Bacillus subtilis. *Proteomics*, **11**, 2992-3001.
22. Savery, N.J. (2007) The molecular mechanism of transcription-coupled DNA repair. *Trends Microbiol*, **15**, 326-333.
23. Epshtein, V. (2015) UvrD helicase: an old dog with a new trick: how one step backward leads to many steps forward. *Bioessays*, **37**, 12-19.
24. Kamarthapu, V. and Nudler, E. (2015) Rethinking transcription coupled DNA repair. *Curr Opin Microbiol*, **24**, 15-20.

25. Savery, N. (2015) A reverse gear for transcription-coupled DNA repair? (Comment on DOI 10.1002/bies.201400106). *Bioessays*, **37**, 4.
26. Guy, C.P., Atkinson, J., Gupta, M.K., Mahdi, A.A., Gwynn, E.J., Rudolph, C.J., Moon, P.B., van Knippenberg, I.C., Cadman, C.J., Dillingham, M.S. *et al.* (2009) Rep provides a second motor at the replisome to promote duplication of protein-bound DNA. *Mol Cell*, **36**, 654-666.
27. Merrikh, C.N., Brewer, B.J. and Merrikh, H. (2015) The B. subtilis Accessory Helicase PcrA Facilitates DNA Replication through Transcription Units. *PLoS Genet*, **11**, e1005289.
28. Boubakri, H., de Septenville, A.L., Viguera, E. and Michel, B. The helicases DinG, Rep and UvrD cooperate to promote replication across transcription units in vivo. *EMBO J*, **29**, 145-157.
29. Harriott, K. The characterisation of the interaction between PcrA and RNA polymerase (2012), PhD thesis, University of Newcastle.
30. Manelyte, L., Guy, C.P., Smith, R.M., Dillingham, M.S., McGlynn, P. and Savery, N.J. (2009) The unstructured C-terminal extension of UvrD interacts with UvrB, but is dispensable for nucleotide excision repair. *DNA Repair*, **8**, 1300-1310.
31. Lee, J.Y. and Yang, W. (2006) UvrD helicase unwinds DNA one base pair at a time by a two-part power stroke. *Cell*, **127**, 1349-1360.
32. Velankar, S.S., Soultanas, P., Dillingham, M.S., Subramanya, H.S. and Wigley, D.B. (1999) Crystal structures of complexes of PcrA DNA helicase with a DNA substrate indicate an inchworm mechanism. *Cell*, **97**, 75-84.
33. Subramanya, H.S., Bird, L.E., Brannigan, J.A. and Wigley, D.B. (1996) Crystal structure of a DExx box DNA helicase. *Nature*, **384**, 379-383.
34. Soultanas, P., Dillingham, M.S., Velankar, S.S. and Wigley, D.B. (1999) DNA binding mediates conformational changes and metal ion coordination in the active site of PcrA helicase. *J Mol Biol*, **290**, 137-148.
35. Stelter, M., Acajjaoui, S., McSweeney, S. and Timmins, J. (2013) Structural and mechanistic insight into DNA unwinding by Deinococcus radiodurans UvrD. *PLoS One*, **8**, e77364.
36. Korolev, S., Hsieh, J., Gauss, G.H., Lohman, T.M. and Waksman, G. (1997) Major domain swiveling revealed by the crystal structures of complexes of E. coli Rep helicase bound to single-stranded DNA and ADP. *Cell*, **90**, 635-647.
37. Smith, A.J. and Savery, N.J. (2005) RNA polymerase mutants defective in the initiation of transcription-coupled DNA repair. *Nucleic Acids Res*, **33**, 755-764.
38. Minor, W., Cymborowski, M., Otwinowski, Z. and Chruszcz, M. (2006) HKL-3000: the integration of data reduction and structure solution--from diffraction images to an initial model in minutes. *Acta Crystallogr D Biol Crystallogr*, **62**, 859-866.
39. Sheldrick, G.M. (2010) Experimental phasing with SHELXC/D/E: combining chain tracing with density modification. *Acta Crystallogr D Biol Crystallogr*, **66**, 479-485.
40. Bricogne, G., Vonrhein, C., Flensburg, C., Schiltz, M. and Paciorek, W. (2003) Generation, representation and flow of phase information in structure determination: recent developments in and around SHARP 2.0. *Acta Crystallogr D Biol Crystallogr*, **59**, 2023-2030.
41. Abrahams, J.P. and Leslie, A.G. (1996) Methods used in the structure determination of bovine mitochondrial F1 ATPase. *Acta Crystallogr D Biol Crystallogr*, **52**, 30-42.
42. Cowtan, K. (2010) Recent developments in classical density modification. *Acta Crystallogr D Biol Crystallogr*, **66**, 470-478.
43. Cowtan, K. (2012) Completion of autobuilt protein models using a database of protein fragments. *Acta Crystallogr D Biol Crystallogr*, **68**, 328-335.
44. Emsley, P., Lohkamp, B., Scott, W.G. and Cowtan, K. (2010) Features and development of Coot. *Acta Crystallogr D Biol Crystallogr*, **66**, 486-501.
45. Vagin, A.A., Steiner, R.A., Lebedev, A.A., Potterton, L., McNicholas, S., Long, F. and Murshudov, G.N. (2004) REFMAC5 dictionary: organization of prior chemical knowledge and guidelines for its use. *Acta Crystallogr D Biol Crystallogr*, **60**, 2184-2195.
46. Adams, P.D., Afonine, P.V., Bunkoczi, G., Chen, V.B., Davis, I.W., Echols, N., Headd, J.J., Hung, L.W., Kapral, G.J., Grosse-Kunstleve, R.W. *et al.* (2010) PHENIX: a comprehensive Python-based system for macromolecular structure solution. *Acta Crystallogr D Biol Crystallogr*, **66**, 213-221.
47. Landau, M., Mayrose, I., Rosenberg, Y., Glaser, F., Martz, E., Pupko, T. and Ben-Tal, N. (2005) ConSurf 2005: the projection of evolutionary conservation scores of residues on protein structures. *Nucleic Acids Res*, **33**, W299-302.

48. Bergendahl, V., Thompson, N.E., Foley, K.M., Olson, B.M. and Burgess, R.R. (2003) A cross-reactive polyol-responsive monoclonal antibody useful for isolation of core RNA polymerase from many bacterial species. *Protein Expr Purif*, **31**, 155-160.
49. Smith, A.J., Szczelkun, M.D. and Savery, N.J. (2007) Controlling the motor activity of a transcription-repair coupling factor: autoinhibition and the role of RNA polymerase. *Nucleic Acids Res*, **35**, 1802-1811.
50. Haines, N.M., Kim, Y.I., Smith, A.J. and Savery, N.J. (2014) Stalled transcription complexes promote DNA repair at a distance. *Proc Natl Acad Sci U S A*, **111**, 4037-4042.
51. Smith, A.J., Pernstich, C. and Savery, N.J. (2012) Multipartite control of the DNA translocase, Mfd. *Nucleic Acids Res*, **40**, 10408-10416.
52. Cole, C., Barber, J.D. and Barton, G.J. (2008) The Jpred 3 secondary structure prediction server. *Nucleic Acids Res*, **36**, W197-201.
53. Kim, D.E., Chivian, D., Malmstrom, L. and Baker, D. (2005) Automated prediction of domain boundaries in CASP6 targets using Ginzu and RosettaDOM. *Proteins*, **61 Suppl 7**, 193-200.
54. Kelley, L.A., Mezulis, S., Yates, C.M., Wass, M.N. and Sternberg, M.J. (2015) The Phyre2 web portal for protein modeling, prediction and analysis. *Nat Protoc*, **10**, 845-858.
55. Stallings, C.L. and Glickman, M.S. (2011) CarD: a new RNA polymerase modulator in mycobacteria. *Transcription*, **2**, 15-18.
56. Sukhodolets, M.V., Cabrera, J.E., Zhi, H. and Jin, D.J. (2001) RapA, a bacterial homolog of SWI2/SNF2, stimulates RNA polymerase recycling in transcription. *Genes Dev*, **15**, 3330-3341.
57. Deaconescu, A.M., Chambers, A.L., Smith, A.J., Nickels, B.E., Hochschild, A., Savery, N.J. and Darst, S.A. (2006) Structural basis for bacterial transcription-coupled DNA repair. *Cell*, **124**, 507-520.
58. Gulten, G. and Sacchettini, J.C. (2013) Structure of the Mtb CarD/RNAP beta-lobes complex reveals the molecular basis of interaction and presents a distinct DNA-binding domain for Mtb CarD. *Structure*, **21**, 1859-1869.
59. Liu, B., Zuo, Y. and Steitz, T.A. (2015) Structural basis for transcription reactivation by RapA. *Proc Natl Acad Sci U S A*, **112**, 2006-2010.
60. Westblade, L.F., Campbell, E.A., Pukhrambam, C., Padovan, J.C., Nickels, B.E., Lamour, V. and Darst, S.A. (2010) Structural basis for the bacterial transcription-repair coupling factor/RNA polymerase interaction. *Nucleic Acids Res*, **38**, 8357-8369.
61. Bae, B., Chen, J., Davis, E., Leon, K., Darst, S.A. and Campbell, E.A. (2015) CarD uses a minor groove wedge mechanism to stabilize the RNA polymerase open promoter complex. *eLife*, **4**.
62. Holm, L. and Rosenstrom, P. (2010) Dali server: conservation mapping in 3D. *Nucleic Acids Res*, **38**, W545-549.
63. Burmann, B.M., Schweimer, K., Luo, X., Wahl, M.C., Stitt, B.L., Gottesman, M.E. and Rosch, P. (2010) A NusE:NusG complex links transcription and translation. *Science*, **328**, 501-504.
64. Musselman, C.A., Avvakumov, N., Watanabe, R., Abraham, C.G., Lalonde, M.E., Hong, Z., Allen, C., Roy, S., Nunez, J.K., Nickoloff, J. *et al.* (2012) Molecular basis for H3K36me3 recognition by the Tudor domain of PHF1. *Nat Struct Mol Biol*, **19**, 1266-1272.
65. Lu, R. and Wang, G.G. (2013) Tudor: a versatile family of histone methylation 'readers'. *Trends Biochem Sci*, **38**, 546-555.
66. Wiedermannova, J., Sudzinova, P., Koval, T., Rabatinova, A., Sanderova, H., Ramaniuk, O., Rittich, S., Dohnalek, J., Fu, Z., Halada, P. *et al.* (2014) Characterization of HelD, an interacting partner of RNA polymerase from Bacillus subtilis. *Nucleic Acids Res*, **42**, 5151-5163.
67. Nudler, E., Avetissova, E., Markovtsov, V. and Goldfarb, A. (1996) Transcription processivity: protein-DNA interactions holding together the elongation complex. *Science*, **273**, 211-217.
68. Mechanic, L.E., Hall, M.C. and Matson, S.W. (1999) Escherichia coli DNA helicase II is active as a monomer. *J Biol Chem*, **274**, 12488-12498.
69. McGlynn, P., Savery, N.J. and Dillingham, M.S. (2012) The conflict between DNA replication and transcription. *Mol Microbiol*, **85**, 12-20.
70. Boubakri, H., de Septenville, A.L., Viguera, E. and Michel, B. (2010) The helicases DinG, Rep and UvrD cooperate to promote replication across transcription units in vivo. *Embo J*, **29**, 145-157.
71. Atkinson, J., Gupta, M.K. and McGlynn, P. (2011) Interaction of Rep and DnaB on DNA. *Nucleic Acids Res*, **39**, 1351-1359.
72. Noirot-Gros, M.F., Dervyn, E., Wu, L.J., Mervelet, P., Errington, J., Ehrlich, S.D. and Noirot, P. (2002) An expanded view of bacterial DNA replication. *Proc Natl Acad Sci U S A*, **99**, 8342-8347.

73. Petit, M.A. and Ehrlich, D. (2002) Essential bacterial helicases that counteract the toxicity of recombination proteins. *Embo J*, **21**, 3137-3147.
74. Taucher-Scholz, G., Abdel-Monem, M. and Hoffmann-Berling, H. (1983) In Cozzarelli, N. R. (ed.), *Mechanism of DNA replication and Recombination*. Liss, New York, pp. 65-76.
75. Mechanic, L.E., Latta, M.E. and Matson, S.W. (1999) A region near the C-terminal end of Escherichia coli DNA helicase II is required for single-stranded DNA binding. *J Bacteriol*, **181**, 2519-2526.
76. Lanouette, S., Mongeon, V., Figeys, D. and Couture, J.F. (2014) The functional diversity of protein lysine methylation. *Mol Syst Biol*, **10**, 724.
77. Schmidt, A., Kochanowski, K., Vedelaar, S., Ahrne, E., Volkmer, B., Callipo, L., Knoops, K., Bauer, M., Aebersold, R. and Heinemann, M. (2016) The quantitative and condition-dependent Escherichia coli proteome. *Nat Biotechnol*, **34**, 104-110.

Figure Legends

Figure 1. The crystal structure of an RNAP interaction domain in PcrA helicase

(A) Crystal structure of the Tudor-like CTD of PcrA. The co-ordinates have been deposited at the PDB under PDB ID code: 5DMA. The structure is coloured according to residue conservation with the least conserved residues in cyan, through white, to most conserved residues in magenta. The protein is shown in ribbons format with side chains only shown for the amino acids which were selected for site-directed mutagenesis studies. (B) A second view of the structure, facing the putative RNAP binding surface. (C) Affinity pulldown assays using the his-tagged proteins indicated as bait and *Bacillus subtilis* cell extract as prey. The upper panel shows an SDS-PAGE gel analysis of the cell extract following pulldown using baited magnetic beads. The bait protein is indicated at the top of the gel and the arrow indicates the position of the β and β′ subunits of RNAP. The lower panel shows western blot analysis of the same gel using a monoclonal antibody against the β subunit of RNA polymerase. In addition to a mock pulldown, the pulldown with ParB (a centromere binding protein that is not known to interact with RNAP) is included as a second negative control for non-specific pulldown of RNAP. (D) Weblogo format multiple sequence alignment of the CTD of ~250 PcrA/UvrD homologues. The residues that were mutated in this study are highlighted using their residue numbers from the *G. stearothermophilus* PcrA protein.

Figure 2. Comparison of Tudor-like domains and their interactions with partner proteins

(A) Structure of the CTD of PcrA (PDB: 5DMA; this work). (B) Superimposition of the RNAP interaction domain of *E. coli* Mfd (cyan) (PDB: 2EYQ; (57)) with a complex between the Mfd

RID (blue) and the β1 domain of RNAP polymerase (brown) (PDB: 3MLQ; (60)). (C) The complex of CarD (red) bound to the RNAP β subunit (brown) (PDB: 4KBM; (58)). (D) Complex between the second Tudor domain of RapA (orange) and the β′ subunit of RNAP (blue) (PDB:4S20; (59)). (E) Complex between the Tudor-like domain of NusG (green) and ribosomal protein s10 (yellow) (PDB:2KVQ; (63)). (F) The PHF1 protein (turquoise) in complex with a peptide (white) shown in stick format and containing a trimethylated lysine residue (red) (PDB:4HCZ; (64)).

Figure 3. Mutation of the PcrA CTD reduces binding to RNA polymerase.

(A) Affinity pulldown assays using the biotinylated proteins as bait and *Bacillus subtilis* cell extract as prey. The upper panel shows an SDS-PAGE gel analysis of the cell extract following pulldown using baited magnetic beads. The arrow signifies the position of the β and β′ subunits of RNAP. The lower panel shows analysis of the same gel using a monoclonal antibody against the β subunit of RNA polymerase. Note that the K712A and L714A mutations were made in the context of full length (FL) PcrA. (B) Quantification of the pulldown experiments using mass spectrometry using the bait proteins indicated and a "no bait" control as the reference. The Relative Ion Score value shown is the total ion score for the prey divided by the equivalent value in the control: a measure of relative abundance of the prey. The enrichment of PcrA in the pulldown samples reflects the presence of the bait protein and acts as an internal control. Selected results are shown for the subunits of RNA polymerase and for several other proteins that are discussed in the text. Further and more detailed results are shown in Supplementary Table 1.

Figure 4. UvrD remodels RNAP transcripts on circular and linear DNA templates

(A) Schematic of the linear and circular DNA templates used for transcription reactions in this work. (B) Remodelling assay for both circular and linear DNA templates as indicated. Reactions were performed either with or without 1 μM UvrD as described in the methods. Biotinylation tags in the template DNA molecules allow the pulldown of the template into a pellet fraction (P) leaving a supernatant fraction (S) which only contains transcripts released into solution. The stall lanes show the stalled transcript product at +20 without the addition of chase nucleotides. All other lanes show transcripts formed following re-initiation of transcription from +20 with a nucleotide chase. Asterisks highlight the position of the principal transcripts that are released into solution by the action of UvrD

Figure 5. Mutation or removal of the CTD reduces UvrD-dependent remodelling of RNAP transcripts, but not DNA translocase activity.

(A) Transcript remodelling assay on linear template DNA. An example gel is shown which has been uniformly contrast enhanced. Lane 1 shows the transcripts arising from the activity of RNAP on a linear DNA construct containing a T7A1 promoter (Figure 4A) in the absence of UvrD. The major product is the result of transcription to the end of the template that results in a 60mer which is indicated on the gel. Lanes 2-5 show the effects of adding increasing concentrations of wild type UvrD (0.05, 0.1, 0.5, 1 μM), resulting in many shorter transcripts in an area of interest marked by the black bar. The bands that are marked with an asterisk are those which are released into free solution by the action of UvrD (see Figure 4 for details). (B) Quantification of the data shown in panel A for the region of interest shown by the black bar. The data were normalized as described in the methods to provide a measure of the RNAP

transcript remodelling activity of the mutant UvrD proteins relative to wild type. The error bars represent the standard error of the mean for six or four independent experiments for wild type or mutant UvrD constructs respectively. (C) The DNA translocase activity of wild type and mutant UvrD proteins was measured with a triplex displacement assay as described in the methods. The error bars represent the standard deviation about the mean for four or three independent experiments for wild type or mutant UvrD constructs respectively.

Sanders et al., Figure 1 revised

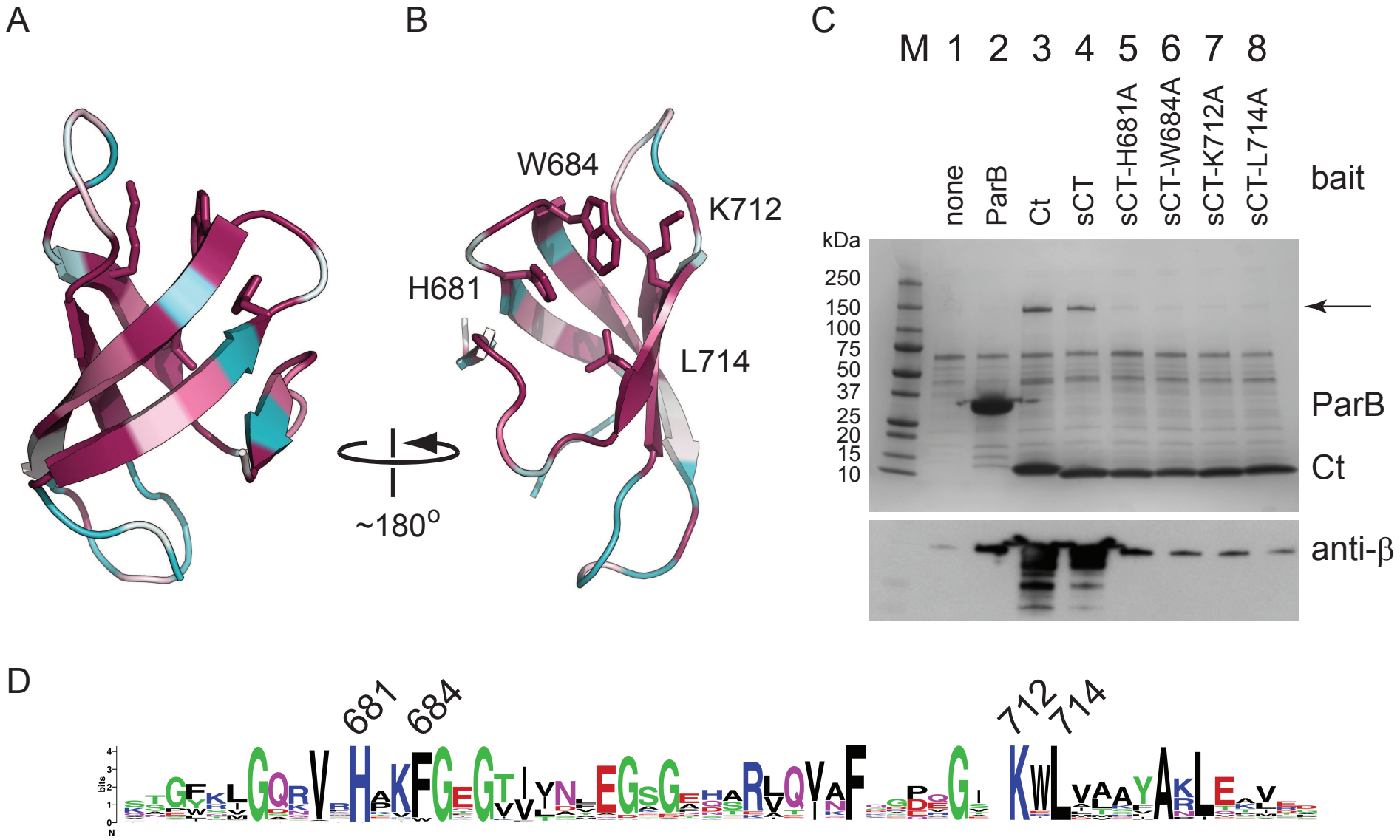

Sanders et al., Figure 2

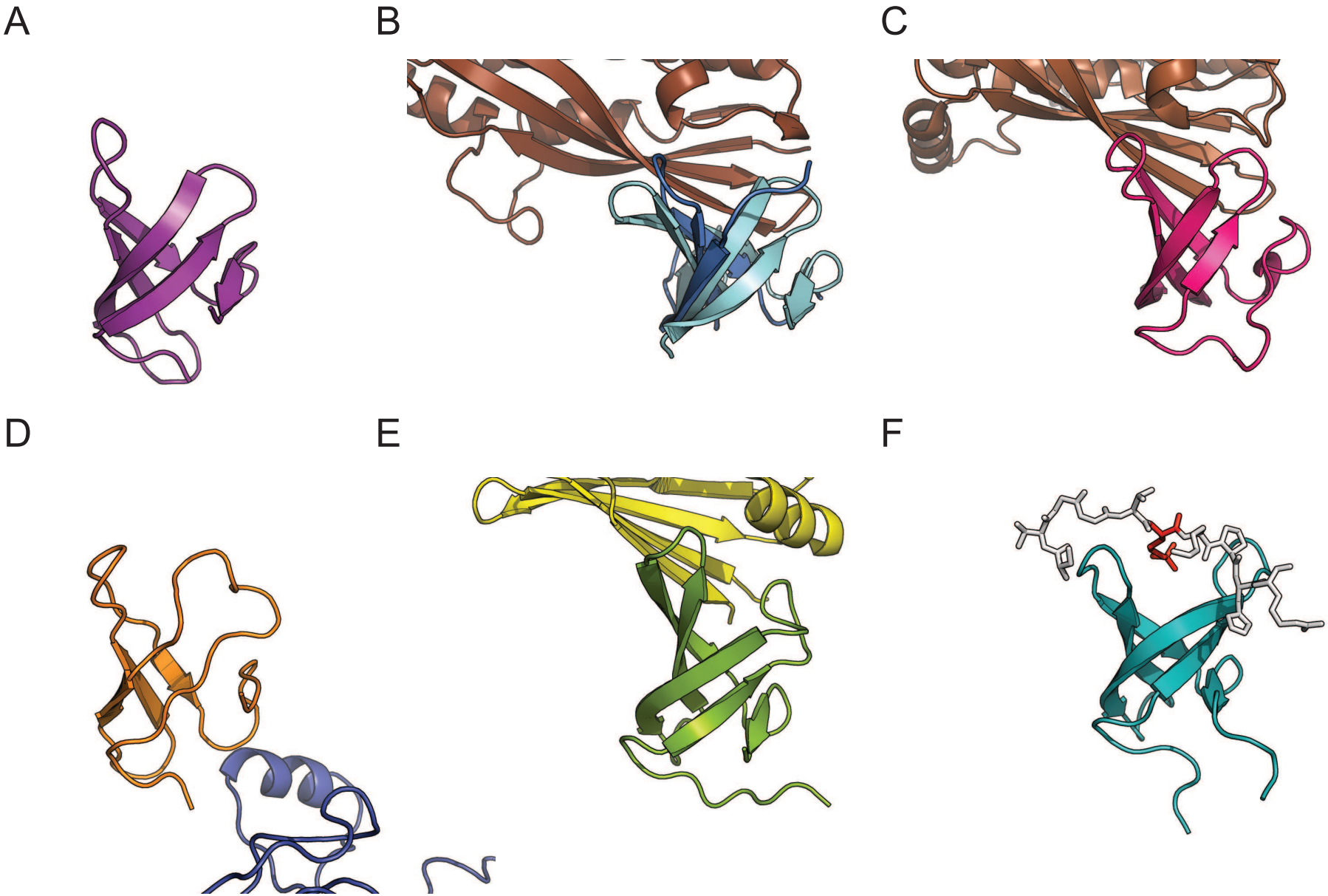

Sanders et al., Figure 3

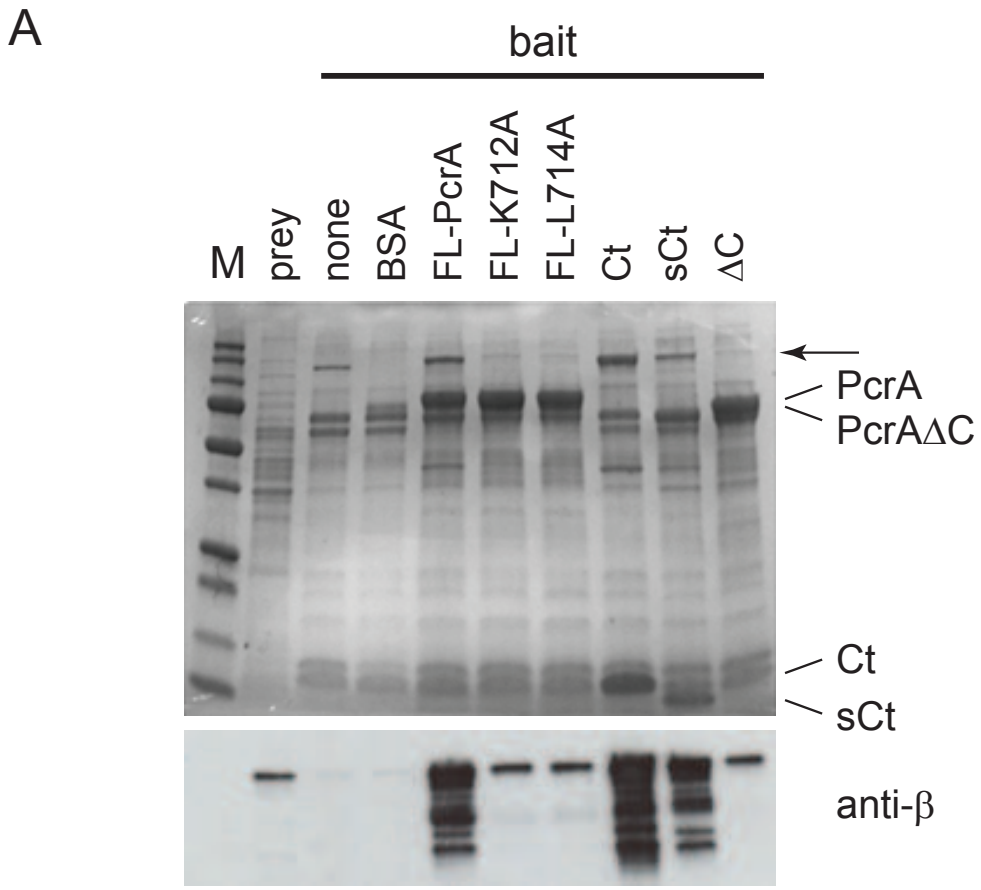

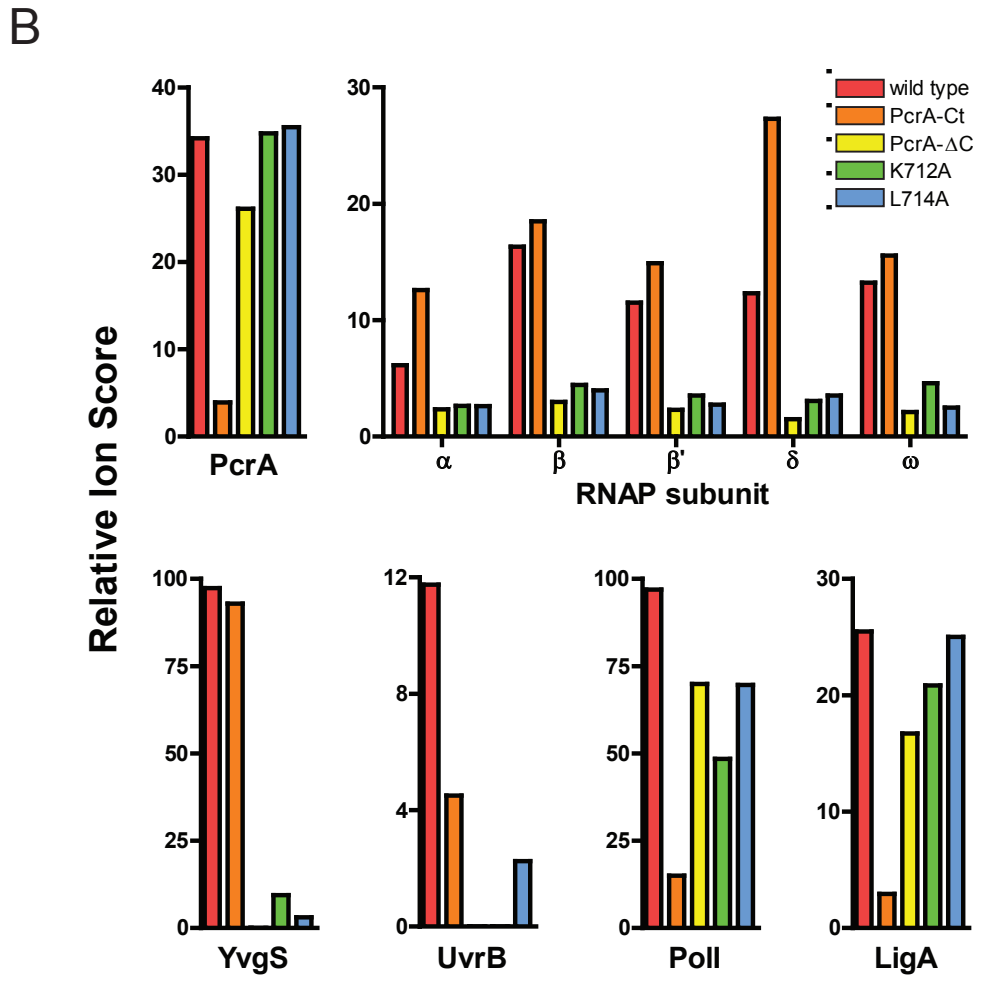

Sanders et al., Figure 4

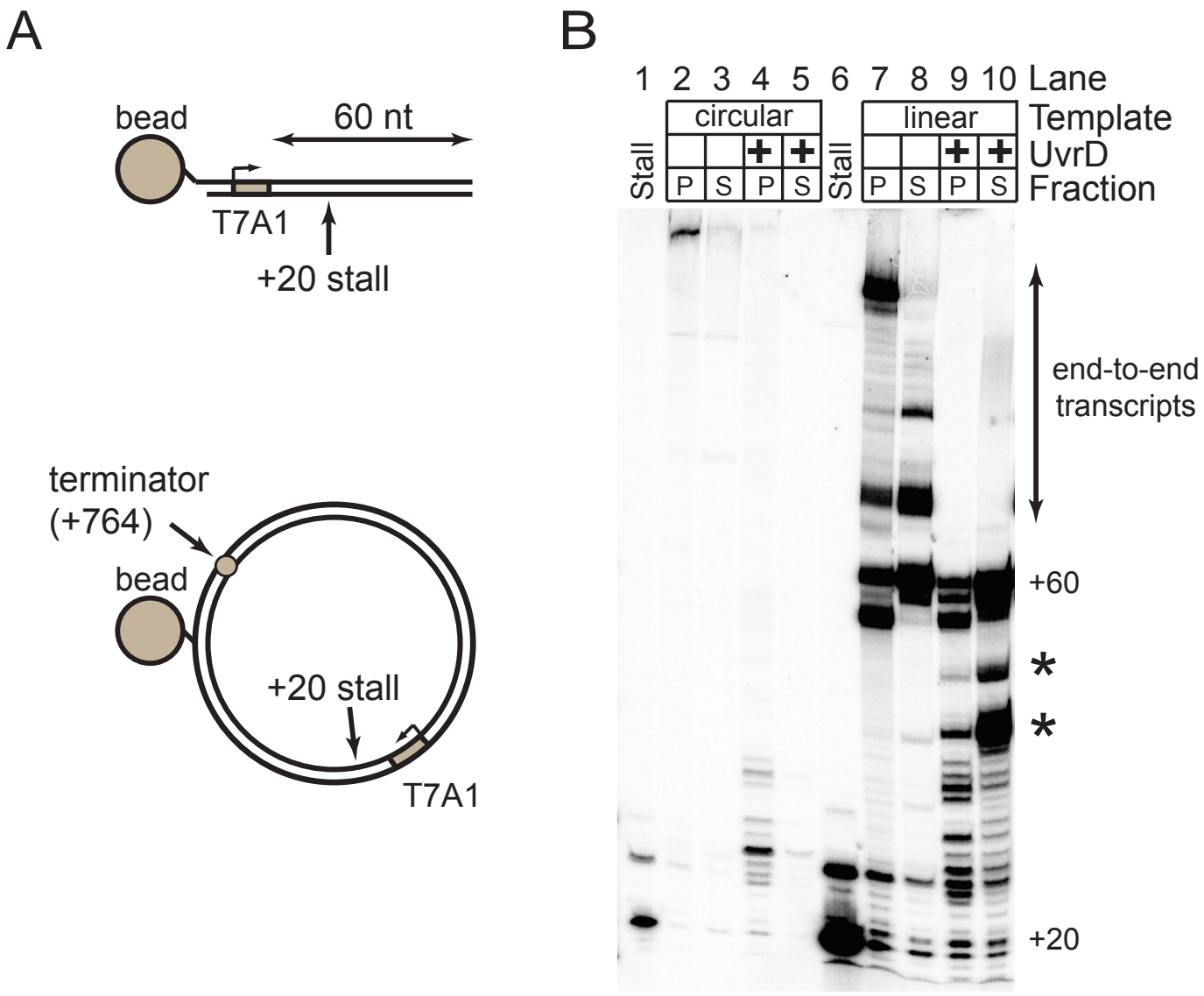

Sanders et al.,Figure 5 revised

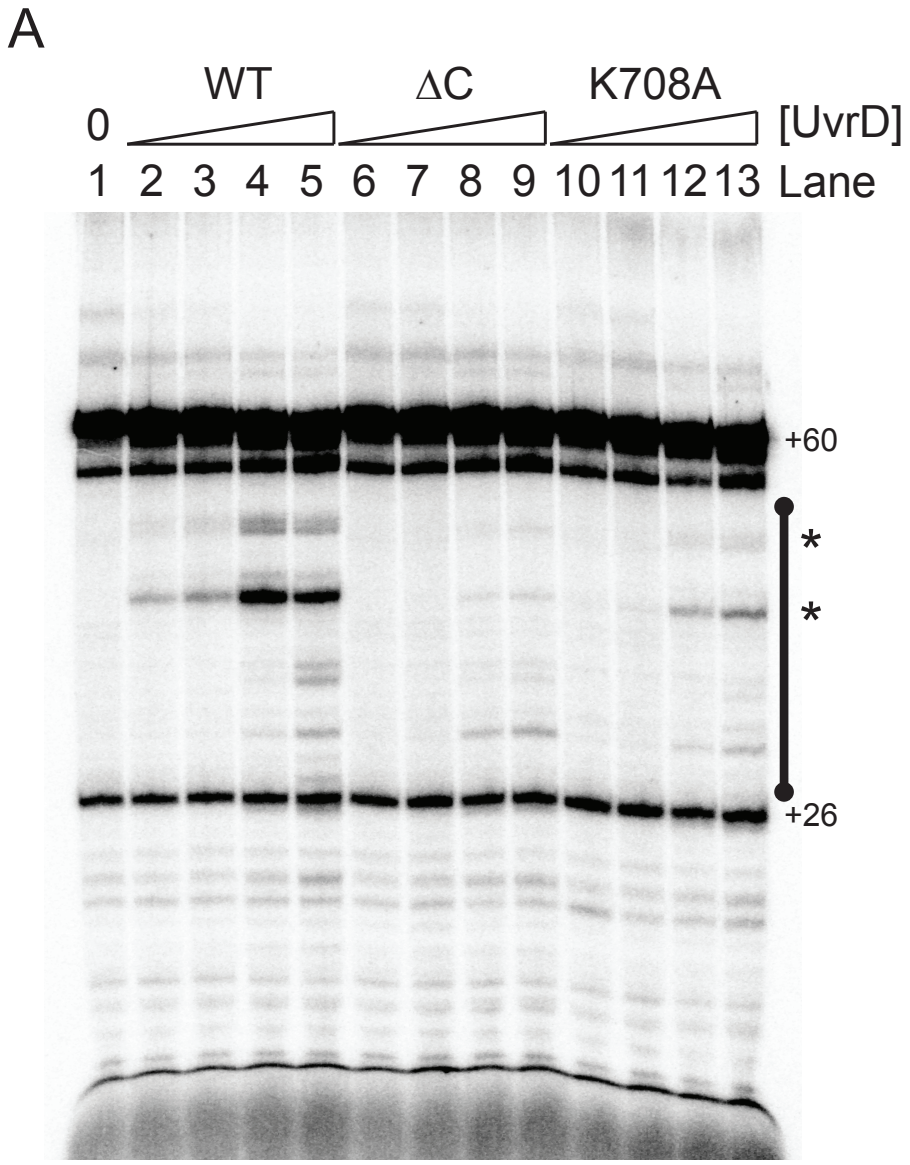

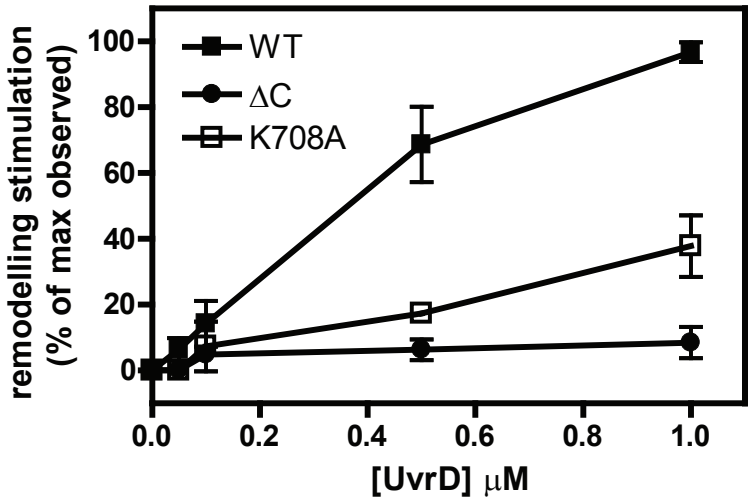

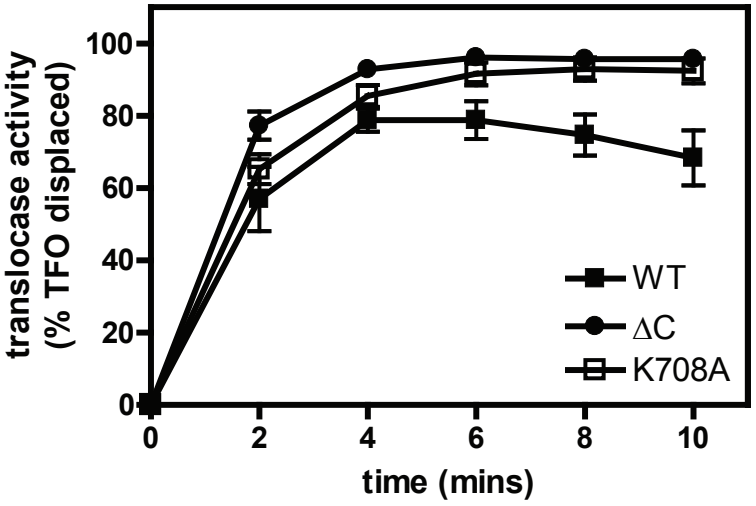

The structure and function of an RNA polymerase interaction domain in the PcrA/UvrD helicase

SUPPLEMENTARY INFORMATION

Sanders, K.*[1], Lin, C-L.*[2], Smith, A.J.*[1], Cronin, N.[2], Fisher, G.[1], Eftychidis., V.[3], McGlynn, P.[3], Savery, N.J.[1], Wigley, D.B.[2] and Dillingham, M.S.[1#]

[1]DNA:Protein Interactions Unit, School of Biochemistry, Biomedical Sciences Building, University of Bristol, BS8 1TD, UK. [2]Institute of Cancer Research, Chester Beatty Laboratories, 237 Fulham Road, London SW3 6JB, UK and Section of Structural Biology, Department of Medicine, Imperial College London, South Kensington Campus, London SW7 2AZ, UK. [3]Department of Biology, University of York, Wentworth Way, York YO10 5DD, United Kingdom.

SUPPLEMENTARY METHODS

Electrophoretic Mobility Shift Assays

The DNA-binding activity of purified PcrA-sCt was analysed by TBE-PAGE gel shift. Serial dilutions of PcrA-sCt, to the indicated concentrations, were incubated with 20 nM radiolabelled substrate (147 base ssDNA oligonucleotide or 147 base pair dsDNA as indicated) in a buffer containing 50 nM HEPES-KOH pH 7.5, 100 mM KCl, 2.5 mM $MgCl_2$, 0.1 mg/mL BSA, 1 mM DTT and 2.5 % (v/v) Ficoll in a 20 µl reaction volume. Samples were incubated at room temperature for 30 mins followed by 5 mins on ice. 10 µl of each were loaded onto a 6% acrylamide/bis-acrylamide (29:1) gel in 90 mM Tris, 150 mM Boric acid (final pH 7.5), 1 mM EDTA. Gels were pre-run at 150 V, 4°C for 30 mins in a buffer identical to their composition, and run post-loading at 150 V, 4°C for 1 hr. For imaging, gels were dried under vacuum and exposed to a phosphor screen, which was subsequently scanned by a Phosphor-Imager (Typhoon FLA 9500, GE Healthcare Life Sciences). ParB protein was used as a positive control for DNA binding.

Circular dichroism spectroscopy

CD spectroscopy was used to assess the folding of wild type and mutant PcrA CTDs. CD spectra were collected at 20^{o}C using a 0.1 cm quartz cuvette in a JASCO J-810 spectropolarimeter. Samples were prepared by dialysing untagged proteins into phosphate buffered saline (PBS, 8.2 mM disodium hydrogen phosphate, 1.8 mM potassium dihydrogen phosphate, 137 mM sodium chloride and 2.7 mM potassium chloride (pH 7.4)) at the concentrations indicated. Data was acquired across a 190-260 nm absorbance scan using a band width of 1.00 nm, time constant of 1

s, scan rate of 100 nm/min, and accumulation of 64 scans, and then normalised to molar ellipticity (MRE (deg.cm^2.dmol^{-1})) by calculation of the concentration of peptide bonds and the cell path length. A buffer only baseline was subtracted from all datasets.

Mass spectrometry sample preparation

Each gel lane was cut into slices and each slice subjected to in-gel tryptic digestion using a ProGest automated digestion unit (Digilab UK). The resulting peptides were fractionated using a Dionex Ultimate 3000 nanoHPLC system in line with an LTQ-Orbitrap Velos mass spectrometer (Thermo Scientific). In brief, peptides in 1% (vol/vol) formic acid were injected onto an Acclaim PepMap C18 nano-trap column (Dionex). After washing with 0.5% (vol/vol) acetonitrile 0.1% (vol/vol) formic acid peptides were resolved on a 250 mm × 75 μm Acclaim PepMap C18 reverse phase analytical column (Dionex) over a 150 min organic gradient, using 7 gradient segments (1-6% solvent B over 1minute, 6-15% B over 58 minutes, 15-32% B over 58 minutes, 32-40% B over 3minutes, 40-90% B over 1minutes, held at 90% B for 6 minutes and then reduced to 1%B over 1 minute.) with a flow rate of 300 nl min^{-1}. Solvent A was 0.1% formic acid and Solvent B was aqueous 80% acetonitrile in 0.1% formic acid. Peptides were ionized by nano-electrospray ionization at 2.1 kV using a stainless steel emitter with an internal diameter of 30 μm (Thermo Scientific) and a capillary temperature of 250°C. Tandem mass spectra were acquired using an LTQ- Orbitrap Velos mass spectrometer controlled by Xcalibur 2.1 software (Thermo Scientific) and operated in data-dependent acquisition mode. The Orbitrap was set to analyze the survey scans at 60,000 resolution (at m/z 400) in the mass range m/z 300 to 2000 and the top twenty multiply charged ions in each duty cycle selected for MS/MS in the LTQ linear ion trap. Charge state filtering, where unassigned precursor ions were not selected

for fragmentation, and dynamic exclusion (repeat count, 1; repeat duration, 30s; exclusion list size, 500) were used. Fragmentation conditions in the LTQ were as follows: normalized collision energy, 40%; activation q, 0.25; activation time 10ms; and minimum ion selection intensity, 500 counts. The raw data files were processed and quantified using Proteome Discoverer software v1.2 (Thermo Scientific) and searched against the UniProt *B.subtilis* database using the SEQUEST (Ver. 28 Rev. 13) algorithm. Peptide precursor mass tolerance was set at 10 ppm, and MS/MS tolerance was set at 0.8 Da. Search criteria included carbamidomethylation of cysteine (+57.0214) as a fixed modification and oxidation of methionine (+15.9949) as a variable modification. Searches were performed with full tryptic digestion and a maximum of 1 missed cleavage was allowed. The reverse database search option was enabled and all peptide data was filtered to satisfy false discovery rate (FDR) of 5%. The Proteome Discoverer software generates a reverse "decoy" database from the same protein database and any peptides passing the initial filtering parameters that were derived from this decoy database are defined as false positive identifications. The minimum cross-correlation factor (Xcorr) filter was readjusted for each individual charge state separately to optimally meet the predetermined target FDR of 5% based on the number of random false positive matches from the reverse decoy database. Thus each data set has its own passing parameters.

Phenotypic analysis of UvrDΔC (UvrD$^{1-647}$)

Sensitivity to UV light was assayed as described (1). The frequency of rifampicin resistant colonies was monitored by inoculating 10 ml of LB with 0.1 ml of an overnight LB culture of the relevant strain and growing with shaking at 37°C to an A650 of 0.4. 10-fold serial dilutions of the culture were made using 56/2 salts and 5 µl of each deletion spotted onto LB plates to

estimate total numbers of colony-forming units/ml after growth overnight at 37°C. Estimation of the numbers of rifampicin resistant colonies was made by plating 100 µl of the mid-log phase culture onto LB containing 15 µg/ml rifampicin. Additionally 1 ml and 5 ml of the same culture were pelleted by centrifugation and each pellet resuspended in 100 µl of 56/2 salts prior to plating out onto LB containing 15 µg/ml rifampicin. Numbers of rifampicin resistant colonies were estimated after overnight growth at 37°C. The fraction of rifampicin resistant colonies was calculated by dividing the number of rifampicin resistant colonies by the total number of colonies after correcting for dilution factors. Viability of *uvrd*/*rep* cells was monitored using a plasmid loss assay as described previously (2). The strains used were: (i) JA031 (pAM403 *(lac*$^{+}$ *rep*$^{+}$*) / ΔlacIZYA uvrD*$^{+}$ *Δrep*::*cat*); (ii) JA033 (pAM403 *(lac*$^{+}$ *rep*$^{+}$*) / ΔlacIZYA ΔuvrD::dhfr Δrep*::*cat*); (iii) VE016 (pAM403 *(lac*$^{+}$ *uvrD*$^{+}$*) / ΔlacIZYA uvrD*$^{1\text{-}647}$::<*kan*> *Δrep*::*cat*).

SUPPLEMENTARY FIGURE LEGENDS

Supplementary Table 1- Mass spectrometry analysis of pulldown experiments using PcrA, PcrA CTD, PcrA ΔCTD, PcrA^{K712A} and PcrA^{L714A} as baits.

Total ion scores are used as a measure of abundance when comparing the same prey protein between datasets. The relative ion score (RIS), which is a measure of relative abundance versus the "no bait" control experiment, is shown for each PcrA bait construct. The RIS columns include a red histogram to highlight the high relative abundance scores. Note that, to aid visualisation of the data, an arbitrary high score of 100 has been used in place of a value of infinity in cases where the prey was not detected in the control. Prey proteins that are discussed in the text are highlighted in yellow. The PcrA detection row (which acts as an internal control because it is detecting the bait protein) is highlighted in green. The table shown here contains data in which the wild type RIS value is >2 and the wild type ion score is >10 in order of descending wild type total ion score. The complete raw datasets for these experiments, including values for the whole proteome and a more detailed account of all the mass spectrometry parameters, are available from the corresponding author upon request.

SFigure 1. Structure of the PcrA/UvrD helicase

(A) Crystal structure of PcrA helicase (3PJR; (3)) colour coded by subdomains according to the key. Note that the CTD (purple) is not observed as it is disordered. (B) Primary structure diagram of PcrA indicating the domain organisation. Numbers indicate the positions of domain boundaries. (C) Sequence alignment of *E. coli* UvrD, *B. subtilis* PcrA and *G. stearothermophilus* PcrA. The alignment is colour-coded according to conservation with darker blue segments more

conserved. Note the high conservation of the final ~50 amino acids that fold into a Tudor-like RNAP interaction domain.

SFigure 2. Purification and RNAP binding ability of the PcrA-sCt protein.

(A) Schematic showing the primary structure of wild type PcrA, his-tagged PcrA-Ct and his-tagged PcrA-sCt proteins. The sequence of the tag is shown and the site of cleavage by HRV 3C protease is marked with an asterisk. (B) SDS-PAGE gel showing purified PcrA-sCt protein with the his-tag either intact or cleaved as indicated. (C) Dose-dependent pulldown of RNAP from *B. subtilis* lysate by the his-tagged PcrA-sCt protein is comparable to that by the his-tagged PcrA-Ct protein, which is equivalent to the construct used in our previous studies (4). The position of the β and β′ subunits of RNAP is indicated with an arrow.

SFigure 3. Purified PcrA-sCt protein does not bind DNA.

Electrophoretic mobility shift assays were performed as described in the methods using *B. subtilis* ParB protein as a positive control. No DNA binding activity was detected for either single- or double-stranded DNA substrates under these conditions at concentrations up to 5 μM PcrA-sCt.

SFigure 4. The CD spectra for wild type and mutant PcrA sCt domains are similar.

Top panel: CD spectra for the proteins indicated were obtained at 0.25 mg/ml as described in the Materials and Methods. The K712A mutant was not available at this concentration. Lower panel: CD spectra for the proteins indicated were obtained at 0.16 mg/ml. All of the spectra are

characteristic of β sheet as expected based on the crystal structure, and suggest that the mutant proteins are globally folded.

SFigure 5. The UvrD-dependent short RNA transcripts that remain associated with the template DNA are backtracked.

Remodelling assays were performed with either wild type UvrD or UvrDΔC, and using GreB to test for backtracking, as described in the main methods section. Lane 1 shows the stalled transcript product (+20) without addition of the chase nucleotides, whereas lanes 2, 3 and 4 show the transcripts formed following re-initiation of transcription using the chase and pulldown with streptavidin beads. Lane 2 shows the total transcript population (T), Lane 3 shows the free RNA transcripts released into the supernatant (S) and lane 4 shows the transcripts that remain associated with RNAP and the DNA template in the pellet (P). Lane 5 shows the effect of treating the pellet fraction with GreB which cleaves any transcripts that are in a backtracked RNAP complex. Lane 6 shows the effect of a 2^{nd} nucleotide chase which will restart transcription following transcript cleavage by GreB. Lane 7 is a control to show the effect of the 2^{nd} chase step but without addition of the GreB factor. Lanes 8-19 show equivalent experiments performed in the presence of wild type UvrD or UvrDΔC. Asterisks highlight the position of the principal transcripts that are released into solution by the action of UvrD. Note that these correspond with the position of prominent cleavage products formed by the action of GreB.

SFigure 6. Deletion of the C-terminal domain of UvrD does not impact on nucleotide excision repair, mismatch repair or the ability of cells to survive in the absence of Rep.

(A) Δ*uvrD* cells display increased sensitivity to 254 nm UV light as compared with *uvrD*$^{+}$ cells due to a defect in nucleotide excision repair (5) (compare also i with ii). In contrast, a chromosomal allele encoding UvrD lacking the C-terminal 73 amino acids, *uvrD*$^{1\text{-}647}$, does not confer increased sensitivity to UV (compare iii with i). This supports the conclusion that UvrD lacking the C-terminus can function in nucleotide excision repair (6) at least up to the highest UV dose tested here. *uvrD*$^{+}$, *uvrD*$^{1\text{-}647}$ and Δ*uvrD* strains are TB28 (MG1655 *ΔlacIZYA uvrD*$^{+}$)(7), N6632 (MG1655 *ΔlacIZYA ΔuvrD::dhfr*)(2) and VE10 (MG1655 *ΔlacIZYA uvrD*$^{1\text{-}647}$*::*<*kan*>). (B) Increased spontaneous acquisition of resistance to rifampicin is conferred by a defect in mismatch repair ability, evinced by the elevated frequency of rifampicin resistant colonies formed by Δ*uvrD* cells as compared with *uvrD*$^{+}$ (8) (compare also i with ii). The frequency of rifampicin resistance in *uvrD*$^{1\text{-}647}$ cells is similar to that of *uvrD*$^{+}$ (compare iii with i), indicating that loss of the UvrD C-terminus does not result in a defect in mismatch repair. The strains used are identical to those in A above. (C) Δ*uvrD* Δ*rep* cells are inviable on rich medium since either Rep or UvrD is needed to act as an accessory replicative helicase to aid fork movement along protein-bound DNA (2,9). Viability can be monitored using a very low copy and highly unstable plasmid, pRC7, that encodes the *lac* operon and either *uvrD* or *rep* (2). Retention or loss of pRC7*rep* can be monitored in strains bearing a chromosomal deletion of the *lac* operon by blue/white screening on LB plates containing X-gal and IPTG (2,7). The instability of pRC7 results in a very high rate of plasmid loss in the absence of antibiotic selection for the plasmid but only if the plasmid-less genotype of the strain confers viability, as for *uvrD*$^{+}$ Δ*rep* cells (2) (see also i). Consequently, Δ*uvrD* Δ*rep* cells cannot lose pRC7*rep* (compare ii with i). In contrast, *uvrD*$^{1\text{-}647}$ Δ*rep* cells can form white plasmidless colonies (iii),

indicating that UvrD lacking the C-terminal domain can compensate for the absence of Rep and confer viability. The strains used are shown in the methods.

References

1. Lloyd, R.G. and Buckman, C. (1991) Genetic analysis of the *recG* locus of *Escherichia coli* K-12 and of its role in recombination and DNA repair. *J. Bacteriol.*, **173**, 1004-1011.
2. Guy, C.P., Atkinson, J., Gupta, M.K., Mahdi, A.A., Gwynn, E.J., Rudolph, C.J., Moon, P.B., van Knippenberg, I.C., Cadman, C.J., Dillingham, M.S. *et al.* (2009) Rep Provides a Second Motor at the Replisome to Promote Duplication of Protein-Bound DNA. *Mol. Cell*, **36**, 654-666.
3. Velankar, S.S., Soultanas, P., Dillingham, M.S., Subramanya, H.S. and Wigley, D.B. (1999) Crystal structures of complexes of PcrA DNA helicase with a DNA substrate indicate an inchworm mechanism. *Cell*, **97**, 75-84.
4. Gwynn, E.J., Smith, A.J., Guy, C.P., Savery, N.J., McGlynn, P. and Dillingham, M.S. (2013) The conserved C-terminus of the PcrA/UvrD helicase interacts directly with RNA polymerase. *PLoS One*, **8**, e78141.
5. Ogawa, H., Shimada, K. and Tomizawa, J. (1968) Studies on radiation-sensitive mutants of *E. coli*. I. Mutants defective in the repair synthesis. *Mol. Gen. Genet.*, **101**, 227-244.
6. Manelyte, L., Guy, C.P., Smith, R.M., Dillingham, M.S., McGlynn, P. and Savery, N.J. (2009) The unstructured C-terminal extension of UvrD interacts with UvrB, but is dispensable for nucleotide excision repair. *DNA Repair (Amst)*, **8**, 1300-1310.
7. Bernhardt, T.G. and de Boer, P.A. (2004) Screening for synthetic lethal mutants in *Escherichia coli* and identification of EnvC (YibP) as a periplasmic septal ring factor with murein hydrolase activity. *Mol. Microbiol.*, **52**, 1255-1269.
8. Viswanathan, M., Burdett, V., Baitinger, C., Modrich, P. and Lovett, S.T. (2001) Redundant exonuclease involvement in Escherichia coli methyl-directed mismatch repair. *J. Biol. Chem.*, **276**, 31053-31058.
9. Boubakri, H., de Septenville, A.L., Viguera, E. and Michel, B. (2010) The helicases DinG, Rep and UvrD cooperate to promote replication across transcription units *in vivo*. *EMBO J.*, **29**.

Sanders et al., Supplementary Table 1

Accession	Description	Control Score	WT Score	WT RIS	CTD Score	CTD RIS	deltaC Score	deltaC RIS	K712A Score	K712A RIS	L714A Score	L714A RIS
P37871	DNA-directed RNA polymerase subunit beta' OS=Bacillus subtilis (strain 168) GN=rpoC PE=1 SV=4 - [RPOC_BACSU]	305.75	3518.07	11.51	4555.28	14.90	703.91	2.30	1081.84	3.54	839.20	2.74
P37870	DNA-directed RNA polymerase subunit beta OS=Bacillus subtilis (strain 168) GN=rpoB PE=1 SV=2 - [RPOB_BACSU]	180.09	2938.50	16.32	3329.66	18.49	537.17	2.98	798.47	4.43	715.37	3.97
O34580	ATP-dependent DNA helicase PcrA OS=Bacillus subtilis (strain 168) GN=pcrA PE=1 SV=1 - [PCRA_BACSU]	39.83	1361.33	34.18	155.88	3.91	1039.72	26.11	1383.22	34.73	1411.15	35.43
P20429	DNA-directed RNA polymerase subunit alpha OS=Bacillus subtilis (strain 168) GN=rpoA PE=1 SV=1 - [RPOA_BACSU]	93.01	569.90	6.13	1170.25	12.58	217.57	2.34	244.99	2.63	243.58	2.62
O32215	Helicase IV OS=Bacillus subtilis (strain 168) GN=helD PE=1 SV=1 - [HELD_BACSU]	3.40	331.03	97.47	315.60	92.93	0.00	0.00	32.44	9.55	10.50	3.09
O34996	DNA polymerase I OS=Bacillus subtilis (strain 168) GN=polA PE=3 SV=1 - [DPO1_BACSU]	3.36	325.52	96.92	50.34	14.99	234.81	69.91	162.82	48.48	233.80	69.61
P05653	DNA gyrase subunit A OS=Bacillus subtilis (strain 168) GN=gyrA PE=1 SV=1 - [GYRA_BACSU]	52.41	325.34	6.21	53.50	1.02	301.23	5.75	218.37	4.17	301.72	5.76
P17820	Chaperone protein DnaK OS=Bacillus subtilis (strain 168) GN=dnaK PE=1 SV=3 - [DNAK_BACSU]	133.04	274.88	2.07	102.79	0.77	226.32	1.70	118.31	0.89	157.68	1.19
O06975	Putative sporulation transcription regulator WhiA OS=Bacillus subtilis (strain 168) GN=whiA PE=3 SV=1 - [WHIA_BACSU]	109.29	225.02	2.06	184.84	1.69	154.66	1.42	252.83	2.31	240.40	2.20
Q45598	Uncharacterized protein YydD OS=Bacillus subtilis (strain 168) GN=yydD PE=4 SV=1 - [YYDD_BACSU]	50.59	185.91	3.67	159.06	3.14	156.12	3.09	294.60	5.82	305.46	6.04
P39138	Arginase OS=Bacillus subtilis (strain 168) GN=rocF PE=1 SV=1 - [ARGI_BACSU]	74.85	181.57	2.43	85.68	1.14	176.12	2.35	77.42	1.03	113.11	1.51
O32210	Glyoxal reductase OS=Bacillus subtilis (strain 168) GN=yvgN PE=1 SV=1 - [GR_BACSU]	67.29	171.84	2.55	56.62	0.84	133.36	1.98	40.90	0.61	83.72	1.24
O07906	Uncharacterized HTH-type transcriptional regulator YraN OS=Bacillus subtilis (strain 168) GN=yraN PE=3 SV=1 - [YRAN_BACSU]	45.63	171.39	3.76	120.55	2.64	111.68	2.45	152.02	3.33	181.29	3.97
P37551	Pur operon repressor OS=Bacillus subtilis (strain 168) GN=purR PE=1 SV=1 - [PURR_BACSU]	5.52	157.76	28.57	73.85	13.38	85.52	15.49	139.19	25.21	147.60	26.73
P80865	Succinyl-CoA ligase [ADP-forming] subunit alpha OS=Bacillus subtilis (strain 168) GN=sucD PE=1 SV=3 - [SUCD_BACSU]	66.73	142.32	2.13	64.29	0.96	157.77	2.36	72.17	1.08	95.64	1.43
O31498	DNA ligase OS=Bacillus subtilis (strain 168) GN=ligA PE=3 SV=1 - [DNLJ_BACSU]	5.33	135.61	25.47	15.64	2.94	89.04	16.72	110.99	20.84	133.16	25.01
P07860	RNA polymerase sigma-F factor OS=Bacillus subtilis (strain 168) GN=sigF PE=1 SV=1 - [RPSF_BACSU]	3.26	117.89	36.17	108.44	33.27	43.09	13.22	41.74	12.80	75.05	23.02
P29072	Chemotaxis protein CheA OS=Bacillus subtilis (strain 168) GN=cheA PE=1 SV=2 - [CHEA_BACSU]	43.20	108.02	2.50	77.80	1.80	75.01	1.74	49.29	1.14	53.91	1.25
O06728	Putative phytoene/squalene synthase YisP OS=Bacillus subtilis (strain 168) GN=yisP PE=1 SV=2 - [YISP_BACSU]	0.00	106.33	100.00	73.85	100.00	34.41	100.00	53.33	100.00	62.18	100.00
Q45595	Putative peptide biosynthesis protein YydG OS=Bacillus subtilis (strain 168) GN=yydG PE=4 SV=1 - [YYDG_BACSU]	51.63	104.44	2.02	226.83	4.39	124.25	2.41	218.82	4.24	176.90	3.43
O34863	UvrABC system protein A OS=Bacillus subtilis (strain 168) GN=uvrA PE=3 SV=1 - [UVRA_BACSU]	16.89	104.15	6.17	57.19	3.39	92.36	5.47	126.33	7.48	169.74	10.05
Q45600	Uncharacterized metallophosphoesterase-like protein YydB OS=Bacillus subtilis (strain 168) GN=yydB PE=3 SV=1 - [YYDB_BACSU]	37.61	102.73	2.73	96.67	2.57	84.99	2.26	165.58	4.40	152.53	4.06
O35011	DNA-directed RNA polymerase subunit omega OS=Bacillus subtilis (strain 168) GN=rpoZ PE=3 SV=1 - [RPOZ_BACSU]	7.41	98.01	13.23	115.19	15.55	15.66	2.11	34.00	4.59	18.44	2.49
P35165	RNA polymerase sigma factor SigX OS=Bacillus subtilis (strain 168) GN=sigX PE=1 SV=2 - [SIGX_BACSU]	2.48	94.69	38.17	55.38	22.32	15.15	6.11	43.35	17.47	53.26	21.47
P94541	Ribonuclease HIII OS=Bacillus subtilis (strain 168) GN=rnhC PE=1 SV=2 - [RNH3_BACSU]	43.94	93.02	2.12	122.49	2.79	73.91	1.68	182.51	4.15	147.25	3.35
P39788	Endonuclease III OS=Bacillus subtilis (strain 168) GN=nth PE=3 SV=1 - [END3_BACSU]	20.78	90.04	4.33	58.62	2.82	87.71	4.22	126.88	6.11	158.72	7.64
O34885	Type-2 restriction enzyme BsuMI component YdiS OS=Bacillus subtilis (strain 168) GN=ydiS PE=2 SV=1 - [YDIS_BACSU]	1.68	88.90	53.02	20.66	12.32	141.56	84.43	180.04	107.38	142.50	84.99
P46337	HTH-type transcriptional regulator IolR OS=Bacillus subtilis (strain 168) GN=iolR PE=3 SV=1 - [IOLR_BACSU]	0.00	88.06	100.00	20.39	100.00	84.25	100.00	113.77	100.00	126.47	100.00
O05389	Uncharacterized oxidoreductase YrbE OS=Bacillus subtilis (strain 168) GN=yrbE PE=3 SV=2 - [YRBE_BACSU]	10.88	87.09	8.00	66.16	6.08	153.52	14.11	91.21	8.38	132.50	12.18
O34705	Phospholipase YtpA OS=Bacillus subtilis (strain 168) GN=ytpA PE=1 SV=1 - [PLBAC_BACSU]	33.06	85.59	2.59	129.29	3.91	66.44	2.01	137.50	4.16	105.78	3.20
P12464	DNA-directed RNA polymerase subunit delta OS=Bacillus subtilis (strain 168) GN=rpoE PE=1 SV=1 - [RPOE_BACSU]	6.86	84.58	12.32	187.43	27.30	10.32	1.50	20.99	3.06	24.20	3.53
P08164	NH(3)-dependent NAD(+) synthetase OS=Bacillus subtilis (strain 168) GN=nadE PE=1 SV=5 - [NADE_BACSU]	34.08	83.36	2.45	21.06	0.62	76.76	2.25	20.97	0.62	47.42	1.39
O31656	Uncharacterized protein YkrK OS=Bacillus subtilis (strain 168) GN=ykrK PE=4 SV=1 - [YKRK_BACSU]	17.63	79.52	4.51	44.14	2.50	51.86	2.94	86.84	4.93	72.51	4.11
P50849	Polyribonucleotide nucleotidyltransferase OS=Bacillus subtilis (strain 168) GN=pnp PE=1 SV=3 - [PNP_BACSU]	29.91	74.99	2.51	24.83	0.83	73.13	2.45	13.87	0.46	20.06	0.67
P12042	Phosphoribosylformylglycinamidine synthase subunit PurL OS=Bacillus subtilis (strain 168) GN=purL PE=1 SV=2 - [PURL_BACSU]	34.63	69.36	2.00	41.75	1.21	54.81	1.58	46.61	1.35	94.16	2.72
P23478	ATP-dependent helicase/nuclease subunit A OS=Bacillus subtilis (strain 168) GN=addA PE=1 SV=2 - [ADDA_BACSU]	0.00	69.21	100.00	39.06	100.00	34.72	100.00	48.97	100.00	74.53	100.00
P17869	RNA polymerase sigma-H factor OS=Bacillus subtilis (strain 168) GN=sigH PE=1 SV=1 - [RPSH_BACSU]	11.33	69.15	6.10	65.06	5.74	9.66	0.85	21.48	1.90	22.78	2.01
O34857	Repressor rok OS=Bacillus subtilis (strain 168) GN=rok PE=1 SV=1 - [ROK_BACSU]	0.00	68.58	100.00	38.63	100.00	53.68	100.00	91.97	100.00	77.07	100.00

P94593	Uncharacterized ATP-dependent helicase YwqA OS=Bacillus subtilis (strain 168) GN=ywqA PE=3 SV=2 - [YWQA_BACSU]	0.00	68.42	100.00	50.74	100.00	18.38	100.00	36.35	100.00	55.32	100.00
O34949	Uncharacterized HTH-type transcriptional regulator YkoM OS=Bacillus subtilis (strain 168) GN=ykoM PE=3 SV=1 - [YKOM_BACSU]	13.92	67.52	4.85	37.16	2.67	115.70	8.31	109.26	7.85	122.50	8.80
O34942	ATP-dependent DNA helicase RecG OS=Bacillus subtilis (strain 168) GN=recG PE=3 SV=1 - [RECG_BACSU]	15.59	65.11	4.18	18.82	1.21	8.38	0.54	53.28	3.42	91.14	5.85
O34384	Uncharacterized protein YceE OS=Bacillus subtilis (strain 168) GN=yceE PE=3 SV=1 - [YCEE_BACSU]	25.15	57.11	2.27	42.09	1.67	47.47	1.89	24.93	0.99	28.89	1.15
P54391	Uncharacterized protein YpiF OS=Bacillus subtilis (strain 168) GN=ypiF PE=4 SV=1 - [YPIF_BACSU]	18.13	56.61	3.12	111.48	6.15	34.82	1.92	49.89	2.75	44.21	2.44
P06574	RNA polymerase sigma-B factor OS=Bacillus subtilis (strain 168) GN=sigB PE=1 SV=3 - [RPSB_BACSU]	7.13	55.80	7.82	82.96	11.63	35.84	5.02	43.76	6.14	45.46	6.37
P29141	Minor extracellular protease vpr OS=Bacillus subtilis (strain 168) GN=vpr PE=1 SV=1 - [SUBV_BACSU]	1.89	54.08	28.67	21.77	11.54	58.83	31.18	123.06	65.23	92.17	48.85
P54616	Enoyl-[acyl-carrier-protein] reductase [NADH] FabI OS=Bacillus subtilis (strain 168) GN=fabI PE=1 SV=2 - [FABI_BACSU]	23.49	53.75	2.29	26.57	1.13	63.25	2.69	21.22	0.90	40.63	1.73
P17922	Phenylalanine--tRNA ligase beta subunit OS=Bacillus subtilis (strain 168) GN=pheT PE=3 SV=2 - [SYFB_BACSU]	16.28	49.85	3.06	14.87	0.91	105.73	6.50	12.43	0.76	9.37	0.58
P94461	Primosomal protein N' OS=Bacillus subtilis (strain 168) GN=priA PE=3 SV=2 - [PRIA_BACSU]	0.00	49.85	100.00	3.58	100.00	26.33	100.00	25.73	100.00	57.50	100.00
O05521	Redox-sensing transcriptional repressor Rex OS=Bacillus subtilis (strain 168) GN=rex PE=1 SV=1 - [REX_BACSU]	8.57	49.24	5.74	12.80	1.49	50.05	5.84	59.25	6.91	57.28	6.68
O34526	Alanine--tRNA ligase OS=Bacillus subtilis (strain 168) GN=alaS PE=3 SV=1 - [SYA_BACSU]	21.39	49.16	2.30	11.17	0.52	99.48	4.65	22.60	1.06	34.41	1.61
Q04778	HTH-type transcriptional regulator AlsR OS=Bacillus subtilis (strain 168) GN=alsR PE=3 SV=1 - [ALSR_BACSU]	0.00	47.16	100.00	9.92	100.00	36.67	100.00	14.55	100.00	12.76	100.00
O34303	Type-2 restriction enzyme BsuMI component YdjA OS=Bacillus subtilis (strain 168) GN=ydjA PE=2 SV=1 - [YDJA_BACSU]	0.00	46.79	100.00	20.22	100.00	22.72	100.00	104.27	100.00	92.33	100.00
O34921	Uncharacterized protein YtoI OS=Bacillus subtilis (strain 168) GN=ytoI PE=3 SV=1 - [YTOI_BACSU]	9.40	45.20	4.81	17.61	1.87	45.88	4.88	90.35	9.61	118.09	12.56
P94463	Methionyl-tRNA formyltransferase OS=Bacillus subtilis (strain 168) GN=fmt PE=3 SV=2 - [FMT_BACSU]	15.82	45.07	2.85	8.46	0.53	37.36	2.36	9.46	0.60	2.18	0.14
O31718	UPF0356 protein YkzG OS=Bacillus subtilis (strain 168) GN=ykzG PE=3 SV=1 - [YKZG_BACSU]	0.00	44.63	100.00	56.89	100.00	7.89	100.00	7.64	100.00	10.03	100.00
P96714	Uncharacterized protein YwqB OS=Bacillus subtilis (strain 168) GN=ywqB PE=3 SV=2 - [YWQB_BACSU]	8.88	43.12	4.86	75.35	8.49	0.00	0.00	77.13	8.69	45.42	5.12
Q45498	UPF0637 protein YktB OS=Bacillus subtilis (strain 168) GN=yktB PE=1 SV=1 - [YKTB_BACSU]	3.02	42.04	13.91	29.80	9.86	50.06	16.57	35.54	11.77	39.74	13.15
P71021	Septum site-determining protein DivIVA OS=Bacillus subtilis (strain 168) GN=divIVA PE=1 SV=1 - [DIV4A_BACSU]	12.05	41.86	3.47	55.10	4.57	56.24	4.67	37.87	3.14	40.92	3.40
O35025	Type-2 restriction enzyme BsuMI component YdiR OS=Bacillus subtilis (strain 168) GN=ydiR PE=2 SV=1 - [YDIR_BACSU]	0.00	41.85	100.00	8.88	100.00	78.47	100.00	116.49	100.00	81.94	100.00
P55873	50S ribosomal protein L20 OS=Bacillus subtilis (strain 168) GN=rplT PE=1 SV=1 - [RL20_BACSU]	17.81	41.59	2.34	83.35	4.68	124.51	6.99	118.06	6.63	118.99	6.68
O06974	Gluconeogenesis factor OS=Bacillus subtilis (strain 168) GN=mgfK PE=3 SV=1 - [GNGF_BACSU]	20.20	41.18	2.04	51.36	2.54	36.83	1.82	51.30	2.54	56.75	2.81
O32236	HTH-type transcriptional repressor RghR OS=Bacillus subtilis (strain 168) GN=rghR PE=1 SV=1 - [RGHR_BACSU]	0.00	40.25	100.00	18.08	100.00	21.13	100.00	13.32	100.00	30.78	100.00
P23477	ATP-dependent helicase/deoxyribonuclease subunit B OS=Bacillus subtilis (strain 168) GN=addB PE=1 SV=2 - [ADDB_BACSU]	0.00	39.24	100.00	6.26	100.00	35.65	100.00	18.81	100.00	37.11	100.00
P13792	Alkaline phosphatase synthesis transcriptional regulatory protein PhoP OS=Bacillus subtilis (strain 168) GN=phoP PE=1 SV=4 - [PHOP_BACSU]	14.25	38.91	2.73	22.33	1.57	20.32	1.43	26.30	1.85	33.34	2.34
P37524	Nucleoid occlusion protein OS=Bacillus subtilis (strain 168) GN=noc PE=1 SV=1 - [NOC_BACSU]	14.86	38.44	2.59	26.73	1.80	41.24	2.77	15.41	1.04	30.22	2.03
P37940	2-oxoisovalerate dehydrogenase subunit alpha OS=Bacillus subtilis (strain 168) GN=bfmBAA PE=1 SV=1 - [ODBA_BACSU]	13.00	37.36	2.87	32.41	2.49	90.69	6.98	62.09	4.78	74.58	5.74
P54476	Probable endonuclease 4 OS=Bacillus subtilis (strain 168) GN=nfo PE=3 SV=1 - [END4_BACSU]	10.21	36.86	3.61	31.77	3.11	34.92	3.42	52.58	5.15	46.66	4.57
P37599	Chemotaxis protein CheV OS=Bacillus subtilis (strain 168) GN=cheV PE=1 SV=1 - [CHEV_BACSU]	10.54	36.19	3.43	9.18	0.87	44.32	4.20	36.86	3.50	20.50	1.94
P39601	Uncharacterized HTH-type transcriptional regulator YwcC OS=Bacillus subtilis (strain 168) GN=ywcC PE=3 SV=2 - [YWCC_BACSU]	13.40	35.00	2.61	42.11	3.14	16.88	1.26	37.55	2.80	27.69	2.07
A3F320	Transcriptional regulator and biotin acetyl-CoA-carboxylase synthetase (Fragment) OS=Bacillus subtilis (strain 168) GN=birA PE=4 SV=1 - [A3F320_BACSU]	4.45	34.96	7.86	7.68	1.73	24.07	5.41	37.16	8.36	39.60	8.90
O32264	Probable 2-ketogluconate reductase OS=Bacillus subtilis (strain 168) GN=yvcT PE=3 SV=1 - [TKRA_BACSU]	16.52	33.71	2.04	11.39	0.69	58.56	3.55	31.12	1.88	23.70	1.44
P10726	RNA polymerase sigma-D factor OS=Bacillus subtilis (strain 168) GN=sigD PE=1 SV=2 - [RPSD_BACSU]	0.00	32.92	100.00	9.73	100.00	6.68	100.00	4.41	100.00	3.98	100.00
P24139	Oligopeptide transport system permease protein OppC OS=Bacillus subtilis (strain 168) GN=oppC PE=2 SV=1 - [OPPC_BACSU]	11.69	32.80	2.81	43.39	3.71	10.39	0.89	19.52	1.67	19.03	1.63
O34635	Probable L-serine dehydratase, beta chain OS=Bacillus subtilis (strain 168) GN=sdaAB PE=3 SV=1 - [SDHAB_BACSU]	2.89	32.22	11.17	17.82	6.18	21.77	7.55	21.54	7.47	27.75	9.62
O34484	Methionine aminopeptidase 2 OS=Bacillus subtilis (strain 168) GN=mapB PE=1 SV=1 - [MAP12_BACSU]	13.42	32.11	2.39	30.17	2.25	34.02	2.54	26.10	1.95	26.33	1.96
P40762	Uncharacterized HTH-type transcriptional regulator YvmB OS=Bacillus subtilis (strain 168) GN=yvmB PE=3 SV=1 - [YVMB_BACSU]	2.18	30.97	14.21	18.18	8.34	10.23	4.69	17.77	8.15	36.13	16.57

P39646	Phosphate acetyltransferase OS=Bacillus subtilis (strain 168) GN=pta PE=1 SV=3 - [PTAS_BACSU]	13.64	30.95	2.27	17.54	1.29	103.29	7.57	21.88	1.60	12.45	0.91
P39118	1,4-alpha-glucan branching enzyme GlgB OS=Bacillus subtilis (strain 168) GN=glgB PE=2 SV=1 - [GLGB_BACSU]	9.07	30.80	3.40	24.62	2.72	11.06	1.22	52.17	5.75	42.29	4.67
P39776	Tyrosine recombinase XerC OS=Bacillus subtilis (strain 168) GN=xerC PE=1 SV=1 - [XERC_BACSU]	6.34	29.94	4.72	12.50	1.97	9.90	1.56	37.02	5.84	55.47	8.75
P39586	Uncharacterized protein YwbC OS=Bacillus subtilis (strain 168) GN=ywbC PE=3 SV=1 - [YWBC_BACSU]	7.80	29.90	3.83	53.85	6.90	9.20	1.18	13.22	1.69	12.60	1.61
P39845	Plipastatin synthase subunit A OS=Bacillus subtilis (strain 168) GN=ppsA PE=1 SV=2 - [PPSA_BACSU]	13.00	29.83	2.29	47.59	3.66	47.74	3.67	16.36	1.26	25.82	1.99
P39610	Pyridoxine kinase OS=Bacillus subtilis (strain 168) GN=pdxK PE=1 SV=1 - [PDXK_BACSU]	13.54	29.30	2.16	7.84	0.58	32.55	2.40	0.00	0.00	19.12	1.41
Q795R8	Uncharacterized protein YtfP OS=Bacillus subtilis (strain 168) GN=ytfP PE=4 SV=2 - [YTFP_BACSU]	8.64	29.28	3.39	54.84	6.34	14.84	1.72	22.74	2.63	18.68	2.16
P81102	Putative NAD(P)H nitroreductase YodC OS=Bacillus subtilis (strain 168) GN=yodC PE=1 SV=3 - [YODC_BACSU]	3.72	29.23	7.87	14.04	3.78	16.99	4.57	19.10	5.14	26.10	7.02
P39914	Uncharacterized protein YtxJ OS=Bacillus subtilis (strain 168) GN=ytxJ PE=4 SV=1 - [YTXJ_BACSU]	2.16	28.77	13.33	7.55	3.50	9.62	4.46	8.03	3.72	3.80	1.76
P80240	Transcription elongation factor GreA OS=Bacillus subtilis (strain 168) GN=greA PE=1 SV=4 - [GREA_BACSU]	11.23	28.68	2.55	33.85	3.01	20.92	1.86	17.06	1.52	19.18	1.71
P14802	Uncharacterized oxidoreductase YoxD OS=Bacillus subtilis (strain 168) GN=yoxD PE=3 SV=2 - [YOXD_BACSU]	8.33	27.69	3.32	35.18	4.22	59.39	7.13	22.87	2.75	32.76	3.93
P54452	Uncharacterized protein YqeG OS=Bacillus subtilis (strain 168) GN=yqeG PE=4 SV=1 - [YQEG_BACSU]	11.15	27.51	2.47	63.11	5.66	20.05	1.80	19.61	1.76	19.16	1.72
P24219	RNA polymerase sigma-54 factor OS=Bacillus subtilis (strain 168) GN=sigL PE=3 SV=1 - [RP54_BACSU]	3.66	27.35	7.48	69.67	19.05	0.00	0.00	13.89	3.80	7.18	1.96
P40737	Antitoxin YxxD OS=Bacillus subtilis (strain 168) GN=yxxD PE=1 SV=1 - [YXXD_BACSU]	7.37	26.91	3.65	20.00	2.71	21.39	2.90	12.51	1.70	4.07	0.55
P96582	HTH-type transcriptional regulator LrpC OS=Bacillus subtilis (strain 168) GN=lrpC PE=1 SV=2 - [LRPC_BACSU]	7.15	26.38	3.69	26.37	3.69	45.27	6.33	48.10	6.73	57.03	7.98
P94443	Negative transcription regulator PadR OS=Bacillus subtilis (strain 168) GN=padR PE=4 SV=1 - [PADR_BACSU]	0.00	25.86	100.00	2.35	100.00	11.61	100.00	15.29	100.00	23.70	100.00
O31796	RNA-binding protein Hfq OS=Bacillus subtilis (strain 168) GN=hfq PE=1 SV=1 - [HFQ_BACSU]	7.90	25.35	3.21	9.08	1.15	40.33	5.11	22.98	2.91	27.70	3.51
P94544	DNA polymerase/3'-5' exonuclease PolX OS=Bacillus subtilis (strain 168) GN=polX PE=1 SV=1 - [POLX_BACSU]	3.86	24.74	6.41	9.00	2.33	55.41	14.35	68.55	17.76	111.78	28.95
P54717	HTH-type transcriptional regulator GlvR OS=Bacillus subtilis (strain 168) GN=glvR PE=2 SV=1 - [GLVR_BACSU]	1.73	23.78	13.78	2.48	1.44	2.39	1.39	22.60	13.10	18.93	10.97
Q45065	Uncharacterized protein YneT OS=Bacillus subtilis (strain 168) GN=yneT PE=4 SV=1 - [YNET_BACSU]	9.64	23.19	2.40	7.26	0.75	26.16	2.71	14.16	1.47	12.12	1.26
P71047	Putative HTH-type transcriptional regulator YwgB OS=Bacillus subtilis (strain 168) GN=ywgB PE=3 SV=1 - [YWGB_BACSU]	9.98	22.88	2.29	13.55	1.36	15.35	1.54	10.23	1.02	18.31	1.83
O34827	Uncharacterized HTH-type transcriptional regulator YkuM OS=Bacillus subtilis (strain 168) GN=ykuM PE=3 SV=1 - [YKUM_BACSU]	1.85	22.77	12.34	5.06	2.74	30.91	16.74	22.25	12.05	35.81	19.40
O07001	Uncharacterized HTH-type transcriptional regulator YvdT OS=Bacillus subtilis (strain 168) GN=yvdT PE=1 SV=1 - [YVDT_BACSU]	10.52	22.26	2.11	10.87	1.03	19.61	1.86	20.82	1.98	18.96	1.80
O31648	Uncharacterized N-acetyltransferase YjdG OS=Bacillus subtilis (strain 168) GN=yjdG PE=3 SV=1 - [YJDG_BACSU]	7.63	22.18	2.91	43.38	5.69	0.00	0.00	7.14	0.94	6.57	0.86
O34357	Thioredoxin-like protein YtpP OS=Bacillus subtilis (strain 168) GN=ytpP PE=2 SV=1 - [YTPP_BACSU]	2.68	22.07	8.25	5.53	2.07	17.39	6.50	15.99	5.97	18.39	6.87
P80871	General stress protein 14 OS=Bacillus subtilis (strain 168) GN=ywrO PE=1 SV=2 - [GS14_BACSU]	5.29	21.80	4.12	3.76	0.71	22.53	4.26	9.05	1.71	7.28	1.38
P36843	Arginine biosynthesis bifunctional protein ArgJ OS=Bacillus subtilis (strain 168) GN=argJ PE=3 SV=2 - [ARGJ_BACSU]	7.87	21.55	2.74	10.08	1.28	15.62	1.98	0.00	0.00	18.34	2.33
O34752	Prolipoprotein diacylglyceryl transferase OS=Bacillus subtilis (strain 168) GN=lgt PE=1 SV=1 - [LGT_BACSU]	0.00	21.44	100.00	22.72	100.00	3.72	100.00	19.51	100.00	6.84	100.00
P32395	Uroporphyrinogen decarboxylase OS=Bacillus subtilis (strain 168) GN=hemE PE=1 SV=1 - [DCUP_BACSU]	9.21	21.10	2.29	22.66	2.46	36.19	3.93	14.67	1.59	14.65	1.59
O34948	Uncharacterized oxidoreductase YkwC OS=Bacillus subtilis (strain 168) GN=ykwC PE=3 SV=1 - [YKWC_BACSU]	9.77	21.05	2.15	15.47	1.58	32.09	3.28	10.82	1.11	25.68	2.63
P39156	Putative sugar phosphate isomerase YwlF OS=Bacillus subtilis (strain 168) GN=ywlF PE=2 SV=1 - [YWLF_BACSU]	1.98	20.41	10.33	5.84	2.96	24.79	12.55	0.00	0.00	3.46	1.75
O32078	Uncharacterized protein YuaE OS=Bacillus subtilis (strain 168) GN=yuaE PE=4 SV=1 - [YUAE_BACSU]	8.26	20.16	2.44	47.65	5.77	56.01	6.78	40.78	4.94	22.92	2.78
P54390	UPF0302 protein YpiB OS=Bacillus subtilis (strain 168) GN=ypiB PE=3 SV=1 - [YPIB_BACSU]	2.13	19.75	9.27	2.81	1.32	15.03	7.05	12.76	5.99	4.42	2.07
O06724	Uncharacterized protein YisK OS=Bacillus subtilis (strain 168) GN=yisK PE=2 SV=1 - [YISK_BACSU]	5.92	19.48	3.29	13.10	2.21	47.90	8.09	14.44	2.44	13.69	2.31
P46354	Purine nucleoside phosphorylase 1 OS=Bacillus subtilis (strain 168) GN=punA PE=1 SV=1 - [PUNA_BACSU]	5.53	19.36	3.50	15.42	2.79	38.11	6.89	16.10	2.91	13.53	2.45
Q45499	Inositol-1-monophosphatase OS=Bacillus subtilis (strain 168) GN=suhB PE=3 SV=1 - [SUHB_BACSU]	1.89	19.35	10.24	4.43	2.34	18.30	9.68	2.07	1.10	6.57	3.47
P94363	Citrate/malate transporter OS=Bacillus subtilis (strain 168) GN=cimH PE=1 SV=1 - [CIMH_BACSU]	6.49	19.31	2.97	7.33	1.13	13.63	2.10	10.44	1.61	19.67	3.03
P37954	UvrABC system protein B OS=Bacillus subtilis (strain 168) GN=uvrB PE=1 SV=2 - [UVRB_BACSU]	1.61	18.92	11.75	7.25	4.50	0.00	0.00	0.00	0.00	3.62	2.25
P96628	Protein SprT-like OS=Bacillus subtilis (strain 168) GN=ydcK PE=3 SV=1 - [SPRTL_BACSU]	7.73	18.65	2.41	27.12	3.51	2.63	0.34	29.11	3.77	23.24	3.01
O31593	Putative efflux system component YhbJ OS=Bacillus subtilis (strain 168) GN=yhbJ PE=3 SV=1 - [YHBJ_BACSU]	7.03	18.39	2.61	5.43	0.77	18.29	2.60	10.80	1.54	3.72	0.53

P39066	Acetoin utilization protein AcuB OS=Bacillus subtilis (strain 168) GN=acuB PE=3 SV=1 - [ACUB_BACSU]	2.65	18.25	6.87	28.04	10.56	14.55	5.48	6.93	2.61	6.05	2.28
P96608	Putative acyl-CoA dehydrogenase YdbM OS=Bacillus subtilis (strain 168) GN=ydbM PE=2 SV=1 - [YDBM_BACSU]	5.10	17.97	3.53	6.44	1.26	36.86	7.23	8.38	1.64	17.45	3.42
O32248	Uncharacterized N-acetyltransferase YvbK OS=Bacillus subtilis (strain 168) GN=yvbK PE=1 SV=1 - [YVBK_BACSU]	8.32	17.81	2.14	19.87	2.39	25.17	3.02	11.55	1.39	19.26	2.31
P32727	Transcription termination/antitermination protein NusA OS=Bacillus subtilis (strain 168) GN=nusA PE=3 SV=2 - [NUSA_BACSU]	6.09	17.63	2.90	10.04	1.65	41.19	6.77	21.03	3.46	25.92	4.26
P71036	Putative HTH-type transcriptional regulator YwnA OS=Bacillus subtilis (strain 168) GN=ywnA PE=1 SV=1 - [YWNA_BACSU]	1.82	17.57	9.67	4.02	2.21	14.46	7.96	14.65	8.07	24.42	13.45
O31737	Uncharacterized protein YlqB OS=Bacillus subtilis (strain 168) GN=ylqB PE=1 SV=1 - [YLQB_BACSU]	0.00	17.54	100.00	14.26	100.00	3.31	100.00	9.74	100.00	7.47	100.00
Q45599	Uncharacterized protein YydC OS=Bacillus subtilis (strain 168) GN=yydC PE=4 SV=1 - [YYDC_BACSU]	3.17	17.52	5.53	5.32	1.68	13.07	4.13	13.83	4.37	11.63	3.67
Q45549	Transcriptional repressor NrdR OS=Bacillus subtilis (strain 168) GN=nrdR PE=3 SV=2 - [NRDR_BACSU]	8.18	16.89	2.06	20.01	2.44	17.50	2.14	16.27	1.99	19.31	2.36
O34305	Uncharacterized protein YtoQ OS=Bacillus subtilis (strain 168) GN=ytoQ PE=4 SV=1 - [YTOQ_BACSU]	3.65	16.71	4.57	5.33	1.46	14.50	3.97	6.20	1.70	8.08	2.21
O07939	Uncharacterized protein YisT OS=Bacillus subtilis (strain 168) GN=yisT PE=3 SV=1 - [YIST_BACSU]	0.00	16.42	100.00	34.42	100.00	10.28	100.00	8.98	100.00	2.98	100.00
O34841	Uncharacterized protein YoeB OS=Bacillus subtilis (strain 168) GN=yoeB PE=1 SV=2 - [YOEB_BACSU]	6.85	16.32	2.38	11.48	1.68	8.38	1.22	16.08	2.35	7.59	1.11
P54159	Uncharacterized protein YpbR OS=Bacillus subtilis (strain 168) GN=ypbR PE=4 SV=1 - [YPBR_BACSU]	5.07	15.80	3.11	5.76	1.14	11.61	2.29	8.37	1.65	0.00	0.00
O07636	Uncharacterized protein YlaL OS=Bacillus subtilis (strain 168) GN=ylaL PE=4 SV=1 - [YLAL_BACSU]	0.00	15.73	100.00	13.61	100.00	21.21	100.00	5.60	100.00	10.19	100.00
O32126	UPF0331 protein YutE OS=Bacillus subtilis (strain 168) GN=yutE PE=1 SV=1 - [YUTE_BACSU]	7.46	15.67	2.10	7.99	1.07	16.79	2.25	7.77	1.04	3.95	0.53
P54512	Transcriptional regulator MntR OS=Bacillus subtilis (strain 168) GN=mntR PE=1 SV=2 - [MNTR_BACSU]	0.00	15.63	100.00	7.06	100.00	3.09	100.00	3.79	100.00	3.78	100.00
P96642	Uncharacterized protein YddE OS=Bacillus subtilis (strain 168) GN=yddE PE=4 SV=1 - [YDDE_BACSU]	3.32	15.49	4.66	6.89	2.08	9.42	2.84	6.79	2.04	7.23	2.18
P37252	Acetolactate synthase small subunit OS=Bacillus subtilis (strain 168) GN=ilvH PE=3 SV=3 - [ILVH_BACSU]	4.41	15.49	3.51	3.16	0.72	3.46	0.78	6.24	1.41	4.53	1.03
P04948	Homoserine kinase OS=Bacillus subtilis (strain 168) GN=thrB PE=3 SV=2 - [KHSE_BACSU]	2.10	15.41	7.34	9.82	4.68	11.38	5.42	15.00	7.15	5.56	2.65
O34381	HTH-type transcriptional regulator PksA OS=Bacillus subtilis (strain 168) GN=pksA PE=3 SV=1 - [PKSA_BACSU]	0.00	15.38	100.00	39.39	100.00	7.60	100.00	11.15	100.00	11.33	100.00
Q796Y8	Putative peroxiredoxin YgaF OS=Bacillus subtilis (strain 168) GN=ygaF PE=3 SV=1 - [BCP_BACSU]	0.00	15.32	100.00	16.39	100.00	21.78	100.00	10.19	100.00	4.94	100.00
O31675	7-cyano-7-deazaguanine synthase OS=Bacillus subtilis (strain 168) GN=queC PE=1 SV=1 - [QUEC_BACSU]	7.50	15.29	2.04	5.69	0.76	8.15	1.09	2.07	0.28	8.49	1.13
P71019	Malonyl CoA-acyl carrier protein transacylase OS=Bacillus subtilis (strain 168) GN=fabD PE=3 SV=2 - [FABD_BACSU]	3.76	15.24	4.05	1.81	0.48	44.93	11.95	5.62	1.50	5.45	1.45
P94588	Uncharacterized protein YwpF OS=Bacillus subtilis (strain 168) GN=ywpF PE=4 SV=1 - [YWPF_BACSU]	5.06	14.90	2.94	27.95	5.52	8.57	1.69	22.82	4.51	13.51	2.67
P94512	Putative uncharacterized hydrolase YsaA OS=Bacillus subtilis (strain 168) GN=ysaA PE=3 SV=2 - [YSAA_BACSU]	4.71	14.63	3.10	0.00	0.00	3.52	0.75	0.00	0.00	2.81	0.60
P50843	4-deoxy-L-threo-5-hexosulose-uronate ketol-isomerase OS=Bacillus subtilis (strain 168) GN=kduI PE=2 SV=1 - [KDUI_BACSU]	5.73	14.41	2.52	0.00	0.00	15.56	2.72	3.46	0.60	0.00	0.00
P71015	HTH-type transcriptional repressor GbsR OS=Bacillus subtilis (strain 168) GN=gbsR PE=3 SV=1 - [GBSR_BACSU]	1.82	14.39	7.90	9.90	5.44	20.25	11.12	16.89	9.27	26.07	14.32
O31504	Putative DNA methyltransferase YeeA OS=Bacillus subtilis (strain 168) GN=yeeA PE=4 SV=1 - [YEEA_BACSU]	0.00	14.20	100.00	4.03	100.00	15.68	100.00	12.29	100.00	35.45	100.00
O31727	UPF0001 protein YlmE OS=Bacillus subtilis (strain 168) GN=ylmE PE=3 SV=1 - [YLME_BACSU]	5.99	14.15	2.36	7.95	1.33	13.86	2.31	0.00	0.00	12.31	2.05
P42976	4-hydroxy-tetrahydrodipicolinate reductase OS=Bacillus subtilis (strain 168) GN=dapB PE=3 SV=2 - [DAPB_BACSU]	6.82	14.01	2.05	7.77	1.14	28.62	4.20	1.78	0.26	11.28	1.65
P45943	Response regulator aspartate phosphatase E OS=Bacillus subtilis (strain 168) GN=rapE PE=3 SV=2 - [RAPE_BACSU]	4.93	13.60	2.76	12.10	2.45	0.00	0.00	35.22	7.15	14.93	3.03
P94559	Putative metallophosphoesterase YsnB OS=Bacillus subtilis (strain 168) GN=ysnB PE=3 SV=2 - [YSNB_BACSU]	0.00	13.59	100.00	22.77	100.00	10.83	100.00	6.93	100.00	10.09	100.00
P55340	Protein EcsB OS=Bacillus subtilis (strain 168) GN=ecsB PE=4 SV=1 - [ECSB_BACSU]	3.88	13.39	3.45	18.57	4.78	0.00	0.00	6.77	1.74	12.48	3.21
O34970	Probable HTH-type transcriptional regulator YttP OS=Bacillus subtilis (strain 168) GN=yttP PE=2 SV=1 - [YTTP_BACSU]	3.75	13.31	3.55	30.70	8.20	0.00	0.00	8.65	2.31	5.70	1.52
P49778	Elongation factor P OS=Bacillus subtilis (strain 168) GN=efp PE=3 SV=2 - [EFP_BACSU]	0.00	13.06	100.00	9.52	100.00	4.51	100.00	9.97	100.00	10.26	100.00
P32730	Uncharacterized protein YlxP OS=Bacillus subtilis (strain 168) GN=ylxP PE=4 SV=1 - [YLXP_BACSU]	0.00	12.97	100.00	13.69	100.00	10.43	100.00	11.04	100.00	10.89	100.00
O34592	AB hydrolase superfamily protein YdjP OS=Bacillus subtilis (strain 168) GN=ydjP PE=2 SV=1 - [YDJP_BACSU]	6.06	12.85	2.12	11.85	1.95	10.97	1.81	2.37	0.39	6.86	1.13
P06567	Primosomal protein DnaI OS=Bacillus subtilis (strain 168) GN=dnaI PE=1 SV=1 - [DNAI_BACSU]	5.14	12.67	2.46	2.26	0.44	0.00	0.00	4.41	0.86	0.00	0.00
P94359	Uncharacterized protein YxkF OS=Bacillus subtilis (strain 168) GN=yxkF PE=4 SV=1 - [YXKF_BACSU]	0.00	12.66	100.00	0.00	100.00	23.04	100.00	13.43	100.00	5.00	100.00
O32044	Single-stranded-DNA-specific exonuclease RecJ OS=Bacillus subtilis (strain 168) GN=recJ PE=3 SV=1 - [RECJ_BACSU]	3.68	12.63	3.43	0.00	0.00	11.59	3.15	5.35	1.45	10.42	2.83
P39694	ComE operon protein 1 OS=Bacillus subtilis (strain 168) GN=comEA PE=1 SV=1 - [COMEA_BACSU]	0.00	12.26	100.00	14.18	100.00	5.56	100.00	25.19	100.00	15.41	100.00

O07624	Uncharacterized beta-barrel protein YwiB OS=Bacillus subtilis (strain 168) GN=ywiB PE=1 SV=1 - [YWIB_BACSU]	0.00	11.98	100.00	8.62	100.00	2.17	100.00	10.26	100.00	6.98	100.00
O34403	Formamidopyrimidine-DNA glycosylase OS=Bacillus subtilis (strain 168) GN=mutM PE=3 SV=4 - [FPG_BACSU]	3.08	11.98	3.88	0.00	0.00	8.99	2.92	10.83	3.51	18.48	5.99
O32253	Central glycolytic genes regulator OS=Bacillus subtilis (strain 168) GN=cggR PE=1 SV=1 - [CGGR_BACSU]	1.66	11.78	7.08	2.35	1.41	29.48	17.72	38.68	23.25	37.74	22.68
P54574	Ferric uptake regulation protein OS=Bacillus subtilis (strain 168) GN=fur PE=1 SV=2 - [FUR_BACSU]	1.90	11.75	6.20	8.91	4.70	10.00	5.27	7.37	3.89	4.74	2.50
P42961	Uncharacterized protein YcsD OS=Bacillus subtilis (strain 168) GN=ycsD PE=3 SV=2 - [YCSD_BACSU]	0.00	11.75	100.00	14.26	100.00	1.81	100.00	3.52	100.00	11.25	100.00
O34527	HTH-type transcriptional regulator CymR OS=Bacillus subtilis (strain 168) GN=cymR PE=1 SV=2 - [CYMR_BACSU]	2.39	11.59	4.85	5.30	2.22	21.35	8.94	12.05	5.04	10.36	4.34
O34331	Putative rRNA methyltransferase YlbH OS=Bacillus subtilis (strain 168) GN=ylbH PE=3 SV=2 - [YLBH_BACSU]	3.20	11.43	3.57	39.99	12.49	24.54	7.66	13.00	4.06	15.98	4.99
O31494	Uncharacterized HTH-type transcriptional regulator YdzF OS=Bacillus subtilis (strain 168) GN=ydzF PE=3 SV=1 - [YDZF_BACSU]	5.36	11.42	2.13	14.47	2.70	1.96	0.37	10.39	1.94	10.14	1.89
O32006	Resolvase homolog YokA OS=Bacillus subtilis (strain 168) GN=yokA PE=3 SV=1 - [YOKA_BACSU]	3.67	11.29	3.07	3.31	0.90	1.97	0.54	38.65	10.52	24.10	6.56
P37568	Transcriptional regulator CtsR OS=Bacillus subtilis (strain 168) GN=ctsR PE=1 SV=1 - [CTSR_BACSU]	3.97	10.74	2.71	10.81	2.72	4.65	1.17	5.35	1.35	4.82	1.21
P96579	Putative ribosomal N-acetyltransferase YdaF OS=Bacillus subtilis (strain 168) GN=ydaF PE=1 SV=1 - [YDAF_BACSU]	0.00	10.54	100.00	9.46	100.00	18.99	100.00	8.88	100.00	2.30	100.00
O34714	Oxalate decarboxylase OxdC OS=Bacillus subtilis (strain 168) GN=oxdC PE=1 SV=1 - [OXDC_BACSU]	3.71	10.37	2.80	4.88	1.32	6.81	1.84	0.00	0.00	1.93	0.52
P37565	33 kDa chaperonin OS=Bacillus subtilis (strain 168) GN=hslO PE=1 SV=1 - [HSLO_BACSU]	2.75	10.35	3.76	0.00	0.00	9.17	3.34	0.00	0.00	2.03	0.74
P70993	Uncharacterized HTH-type transcriptional regulator YwhA OS=Bacillus subtilis (strain 168) GN=ywhA PE=3 SV=1 - [YWHA_BACSU]	0.00	10.33	100.00	6.43	100.00	23.34	100.00	17.88	100.00	28.87	100.00
O07617	Uncharacterized phosphatase PhoE OS=Bacillus subtilis (strain 168) GN=phoE PE=3 SV=1 - [PHOE_BACSU]	1.86	10.29	5.55	6.34	3.42	14.37	7.75	3.77	2.03	8.29	4.47
P54591	Uncharacterized ABC transporter ATP-binding protein YhcG OS=Bacillus subtilis (strain 168) GN=yhcG PE=3 SV=1 - [YHCG_BACSU]	0.00	10.29	100.00	5.70	100.00	17.01	100.00	11.59	100.00	10.33	100.00
P94352	Uncharacterized protein YxjI OS=Bacillus subtilis (strain 168) GN=yxjI PE=3 SV=1 - [YXJI_BACSU]	3.32	10.24	3.09	13.38	4.04	7.67	2.31	4.82	1.45	6.83	2.06
P81101	Ribosome-recycling factor OS=Bacillus subtilis (strain 168) GN=frr PE=1 SV=2 - [RRF_BACSU]	3.59	10.22	2.85	15.50	4.32	28.96	8.08	6.45	1.80	6.48	1.81
P40400	Putative aliphatic sulfonates-binding protein OS=Bacillus subtilis (strain 168) GN=ssuA PE=2 SV=1 - [SSUA_BACSU]	3.67	10.16	2.77	4.39	1.20	0.00	0.00	0.00	0.00	0.00	0.00
P54389	TPR repeat-containing protein YpiA OS=Bacillus subtilis (strain 168) GN=ypiA PE=3 SV=1 - [YPIA_BACSU]	0.00	10.03	100.00	105.97	100.00	3.82	100.00	1.90	100.00	3.68	100.00
P94548	Fatty acid metabolism regulator protein OS=Bacillus subtilis (strain 168) GN=fadR PE=1 SV=1 - [FADR_BACSU]	1.69	10.03	5.94	8.26	4.90	3.64	2.16	2.54	1.50	4.37	2.59

Sanders et al., Supplementary Figure 1

A

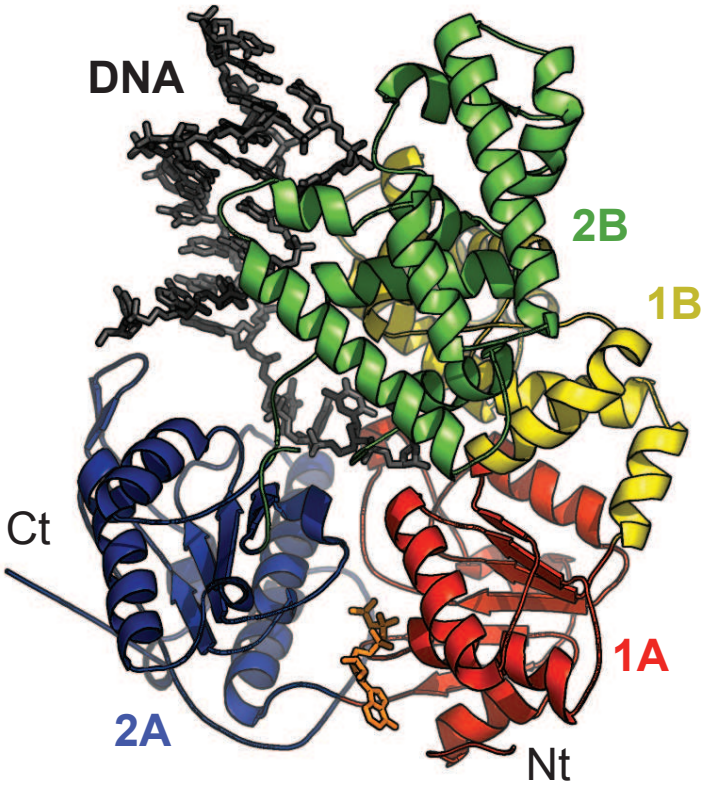

B

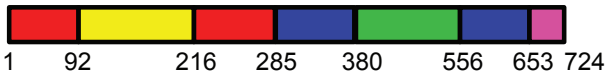

C

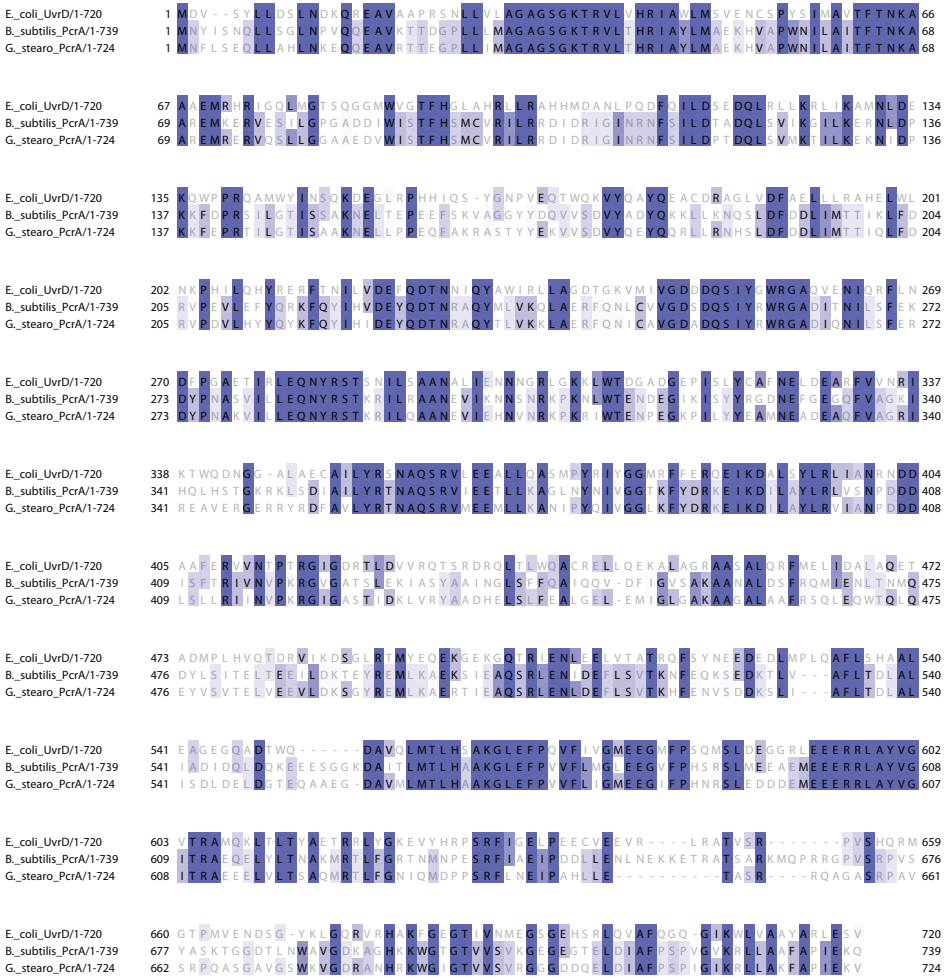

Sanders et al., Supplementary Figure 2

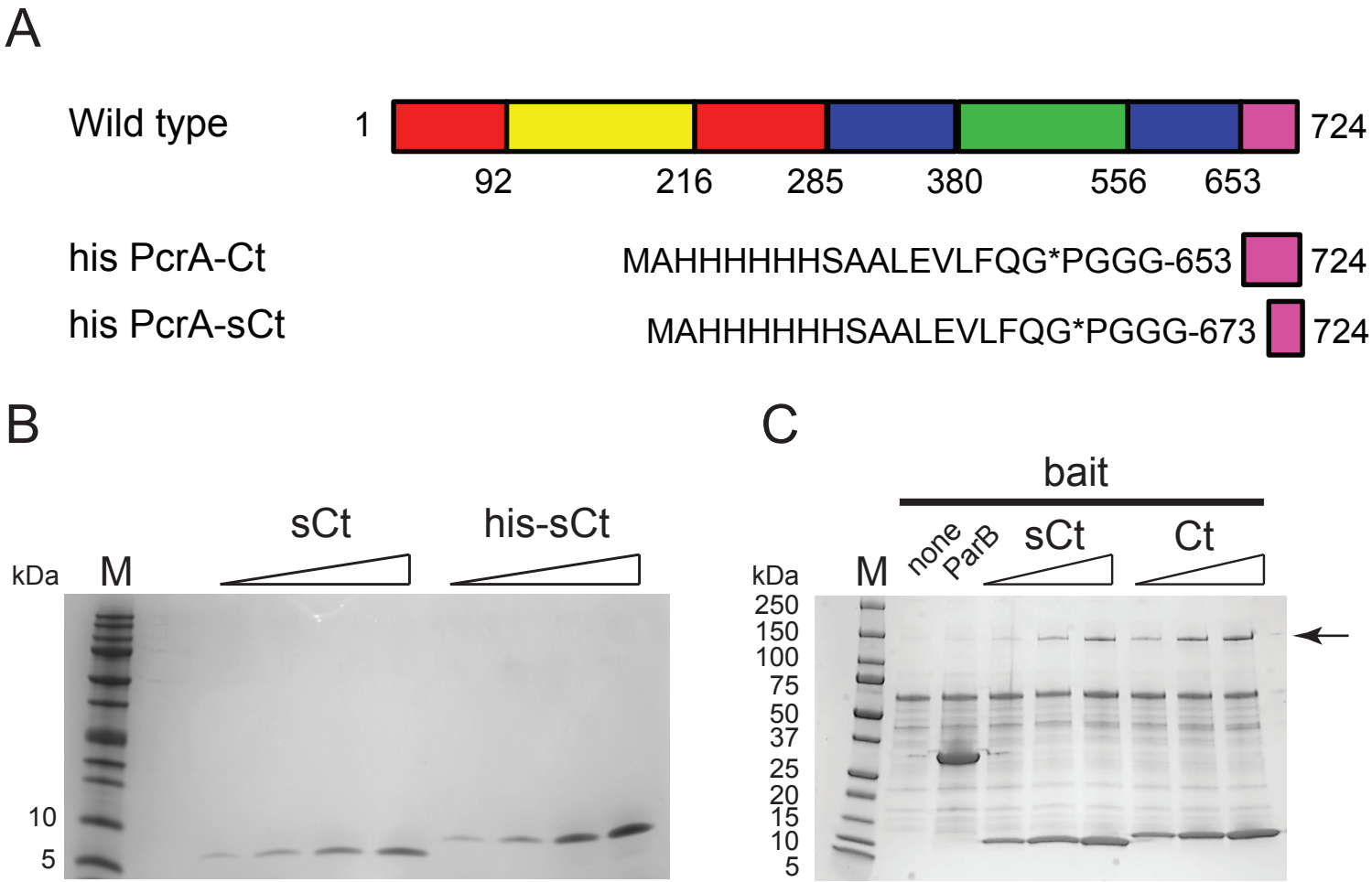

Sanders et al., Supplementary Figure 3

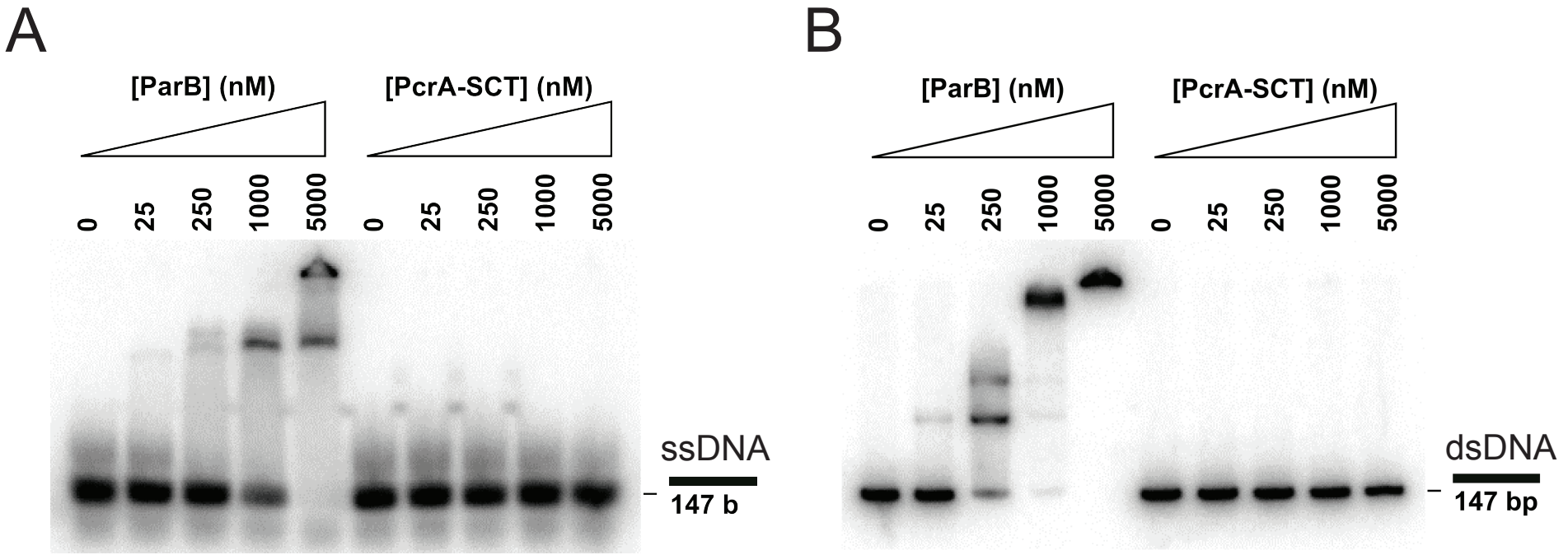

Sanders et al., Supplementary Figure 4

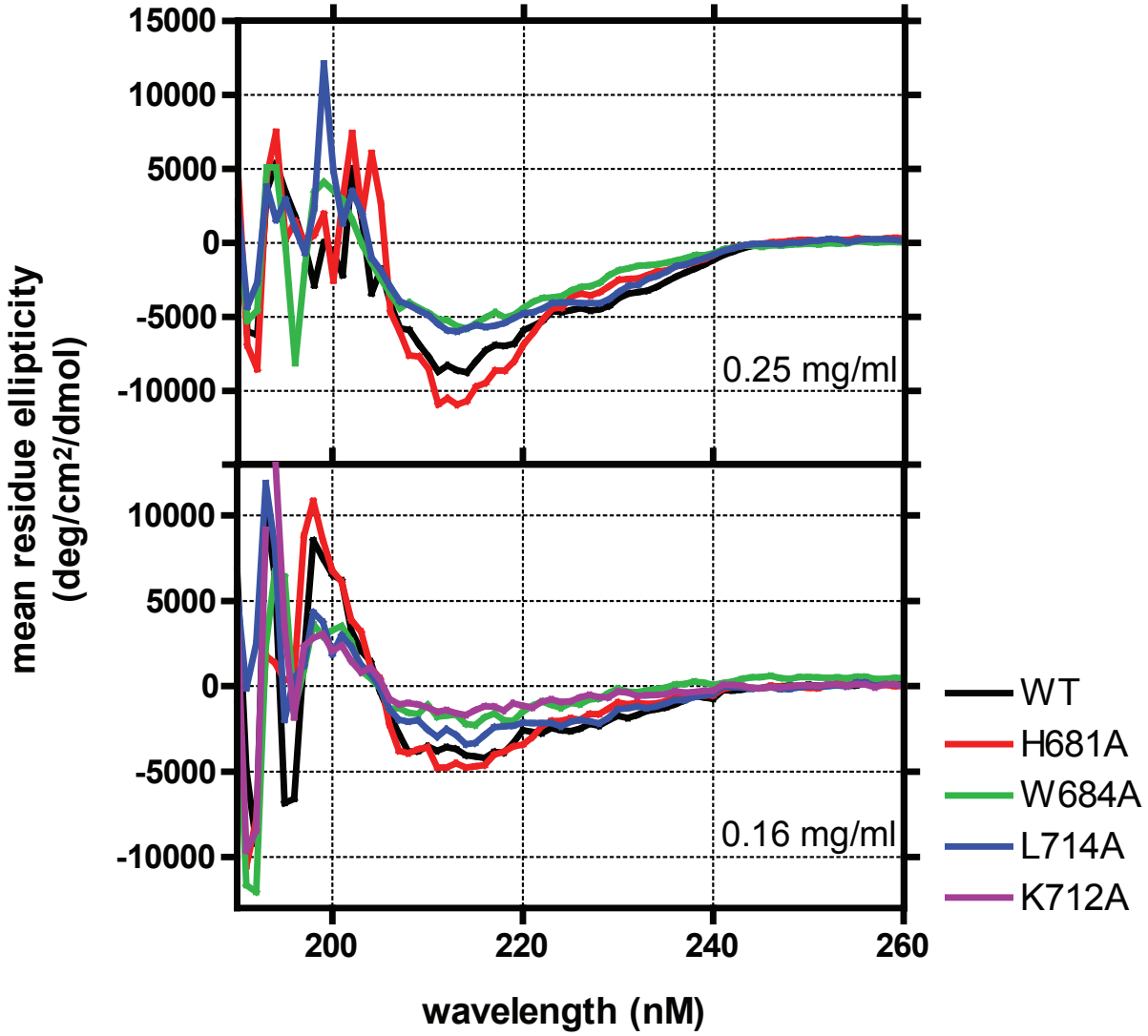

Sanders et al., Supplementary Figure 5

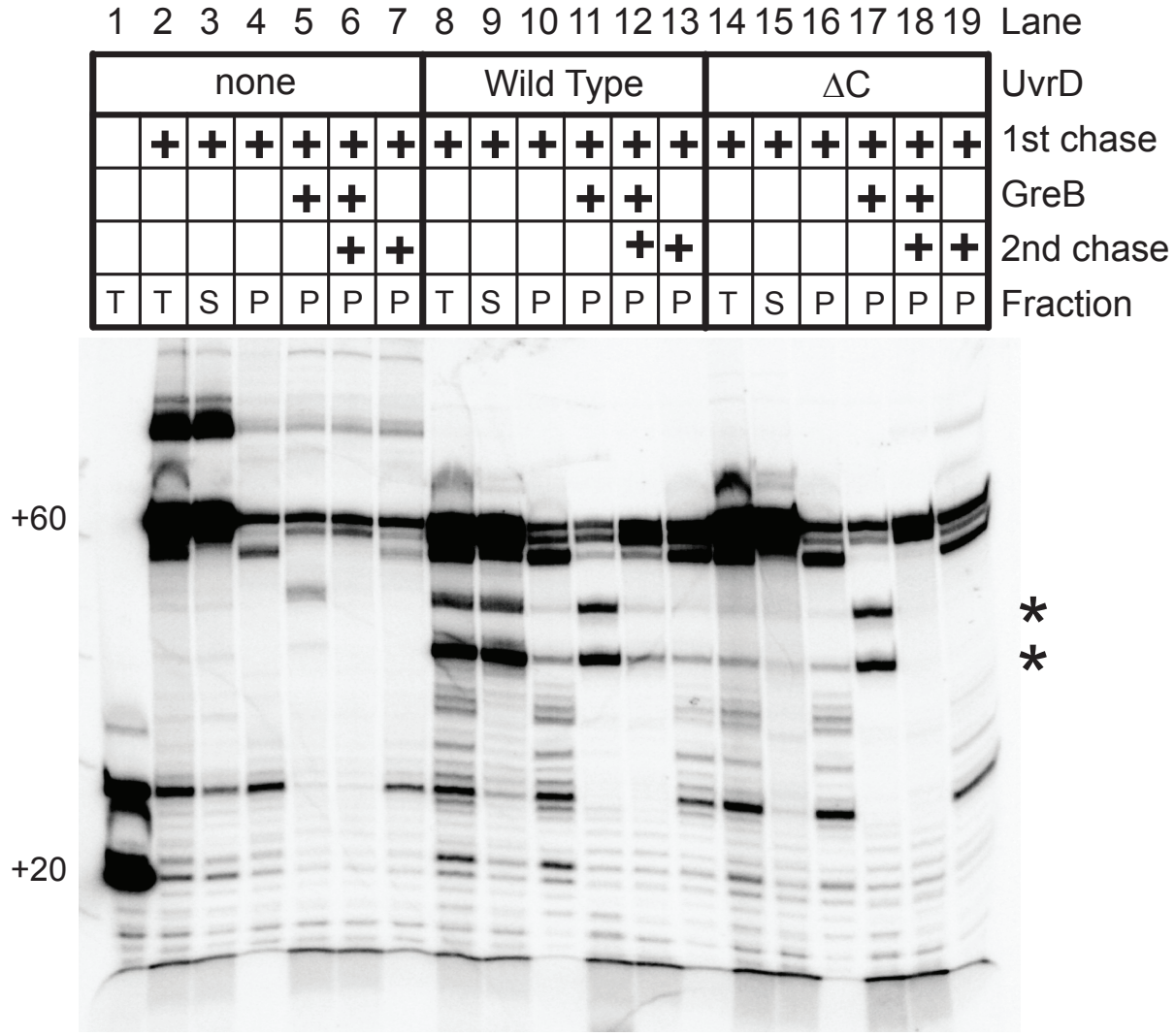

Sanders et al., Supplementary Figure 6